NOVA SCHOOL OF SCIENCE & TECHNOLOGY

PHYSICS DEPARTMENT

TIAGO MARQUES LEVY LIMA

BSc in Biotechnology

MACROPHAGE RESPONSE TO THE INCORPORATION OF DOPED BIO-ACTIVE GLASS IN A BONE REGENERATION SCAFFOLD

MASTER IN BIOMATERIALS AND NANOMEDICINE

NOVA University Lisbon

September, 2024

NOVA SCHOOL OF SCIENCE & TECHNOLOGY

PHYSICS DEPARTMENT

Macrophage response to the incorporation of doped bioactive glass in a bone regeneration scaffold

TIAGO MARQUES LEVY LIMA

BSc in Biotechnology

Adviser: Jorge Alexandre Monteiro de Carvalho e Silva,
Associate Professor, NOVA FCT

Co-advisers: Ana Sofia Pádua,
Phd Student, NOVA FCT

Examination Committee:

Chair: Luís Alexandre Almeida Fernandes Cobra Branco,
Associate Professor, NOVA FCT

Rapporteurs: Maria do Carmo Henriques Lança,
Auxiliary Professor, NOVA FCT

Adviser: Jorge Alexandre Monteiro de Carvalho e Silva,
Associate Professor, NOVA FCT

Members:

MASTER IN BIOMATERIALS AND NANOMEDICINE

NOVA University Lisbon
September, 2024

Macrophage Response to the incorporation of doped bio-active glass in a bone regeneration scaffold.

For my friends and family that give joy to my life.

ACKNOWLEDGMENTS

First and foremost I would like to thank all of my friends and family for accompanying me throughout my life and while I completed my master's thesis. They provided me with unconditional support, gave me the best advice, and made me feel loved and motivated whilst finishing this important step of my life.
I would like to express my gratitude to my coordinator, Prof. Dr. Jorge Carvalho Silva, for presenting me with the opportunity to work with him and to have him as my coordinator. I would like to thank my co-coordinator, Ana Sofia Pádua, for guiding me on the procedures that I made, for answering my questions, for sharing your knowledge with me, for correcting the mistakes that I made, and for her availability.
I would also like to thank Dr. Tânia Santos Vieira for helping me when I had doubts regarding certain procedures and for being a great individual who brightened the mood of the laboratory.

“Simply Lovely.”
(Max Verstappen).

ABSTRACT

Bones make up our skeleton and have several essential roles in the body. Most minor bone fractures or defects heal without any major intervention. However, large bone damages lack this self-regeneration ability and require surgical intervention. Given the pressing clinical need, the market for biomaterials-based treatment for bone repair is growing at a fast rate. In the case of bone repair, scaffolds require certain desirable properties in order to be effective, such as osteoinductivity, osteoconductivity, capable of osseointegration and prevent pro-inflammatory responses, but they should also be rigid and resilient since they will act as the main supporting framework of bone graft, while simultaneously have a porous morphology. Bioglasses are one of the best biomaterials in terms of rates of bioactivity, which allows for the formation of a layer of hydroxyapatite that possesses a chemical phase and structure close to the mineral composition of bones. The presence of species of niobium (Nb) in biomaterials has been shown to improve their mechanical and bioactive properties, having been reported that Nb ions promote the mineralization and differentiation of osteogenic cells. The insertion of niobium in ceramic matrices has also shown great corrosion resistance and very low cytotoxicity. In this work, PCL scaffolds (PCLs), 45S5 BG-PCL scaffolds (45S5BGs), and Nb4%BG-PCL scaffolds (Nb4%BGs) were produced. These composite scaffolds present a porous network in their internal structure, with the BG scaffolds' pores around 140 μm which is suitable for cell infiltration and growth. The addition of Nb to the Bioglass did not result in modifications to its network. The passivated (P) scaffolds and BG had more Saos-2 cell viability than the non-passivated (NP) scaffolds and BG. Nb4%s and powder had more Saos-2 cell viability than 45S5BGs and powder. None of the scaffolds appear to have any anti-bacterial activity. PCLs showed the highest rate of adhesion and proliferation, followed by Nb4%s and 45S5BGs appear to negatively affect the adhesion and proliferation of Saos-2 cells. Nb4%s present higher ALP production, followed by PCLs and 45S5BGs appear to be a hindrance to the production of ALP. Nb4%BG samples present results that show that they improve THP-1 cell growth and viability, having achieved more than 100% cell survivability. Both 45S5BGs and Nb4%s were shown to induce M2 macrophage polarization.

Keywords: Bioglass®, Niobium, Scaffold, Bone Tissue Engineering, Bioactivity, Macrophage Polarization

RESUMO

Os ossos compõem o nosso esqueleto e desempenham varias funções-chave. A maioria das fracturas leves regeneram sem intervenção severa. Mas, danos ósseos severos não possuem esta habilidade, requerendo intervenção cirúrgica. No caso de reparação óssea, as scaffolds requerem várias propriedades, como a osteoinductividade, osteocondutividade, a capacidade para a osteointegração, prevenirem respostas pró-inflamatórias, possuir uma morfologia porosa, enquanto sendo rígidas e resilientes. Os biovidros são uns dos melhores biomateriais em termos de bioactividade, o que permite a formação de uma camada de hydroxyapatite, que apresenta uma estrutura e fase química semelhante à composição mineral dos ossos. Tem sido relatado que a presença de nióbio (Nb) em biomateriais promove as suas propriedades bioactivas e mecânicas, e que os iões de niobio promove a diferenciação e mineralização de celulas osteogénicas. A inserção de nióbio em ligas metálicas e matrizes de cerâmica demonstrou superior resistência a corrosão e baixa citotoxicidade. Neste trabalho, scaffolds de PCL (PCLs), scaffolds de 45S5 BG-PCL (45S5BGs) e scaffolds de Nb4%BG-PCL (Nb4%BGs) foram produzidas. As scaffolds apresentam uma rede porosa, com os poros das scaffolds com BG tendo um tamanho de cerca de 140 µm, o que é adequado para infiltração e crescimento celular. A adição de nióbio ao biovidro não resultou em nenhuma modificação à sua estrutura. As scaffolds passivadas e pó de biovidro obtiveram melhor viabilidade de células Saos-2 do que as scaffolds não passivadas e pó de biovidro. As Nb4BG%s e o pó do mesmo BG obtiveram melhor viabilidade de células Saos-2 do que as 45S5BGs. Nenhuma das scaffolds apresentou actividade antibacteriana. As scaffolds de PCL demonstraram melhores resultados de adesão e proliferação, seguidas das Nb4%BGs e as 45S5BGs demonstraram afectar negativamente a adesão e proliferação das células Saos-2. As Nb4%s apresentaram produção de ALP mais elevada, seguidas pelas PCLs e as 45S5BGs demonstram afectar negativamente a produção de ALP. As amostras de Nb4% demonstrar melhorar o crescimento celular e viabilidade de células THP-1 tendo obtido resultados superiores a 100% sobrevivência celular. Ambas as 45S5BGs e Nb4%s demonstraram induzir polarização de macrófagos do fenótipo M2.

Palavras chave: Biovidro®, Nióbio, Scaffold, Engenharia de tecidos ósseos, Polarização de macrofagos

CONTENTS

LIST OF FIGURES

LIST OF TABLES

ACRONYMS

ALP	Alkaline phosphatase.
BG	45S5 Bioglass®
BMP	Bone morphogenetic protein
BMSC	Bone marrow-derived mesenchymal stem cell
BSA	Bovine serum albumin
BTE	Bone tissue engineering
DAPI	4',6-Diamidino-2-phenylindole.
DMSO	Dimethyl sulfoxide.
E.Coli	Escherichia coli
ECM	Extracellular matrix
FDA	Federal drug administration
FGF	Fibroblast growth factor
FTIR	Fourier-transform infrared spectroscopy
GF	Growth Factor
HA	Hydroxyapatite
HCA	Hydroxycarbonate apatite
IFN- γ	Interferon- γ
IL	Interleukins
iNOS	Inducible nitric oxide synthase
LPS	Lipopolysaccharide

MCS	Mesenchymal Stem Cells
MRSA	Methicillin-resistant Staphylococcus aureus
Nb	Niobium
NO	Nitric Oxide
PBS	Phosphate-buffered saline
PCL	Poly-caprolactone
PDGF	Platelet-derived growth factor
PFA	Paraformaldehyde
PGA	Polyglycolic acid
PLA	Polylactic acid
PLGA	Polylactic-co-glycolic acid
PMA	Phorbol-12-myristate-13-acetate
PNPP	p-Nitrophenyl Phosphate
RPMI	Roswell Park Memorial Institute
SBF	Simulated body fluid
SEM	Scanning electron microscopy
SEM-EDS	Scanning electron microscopy and energy-dispersive X-ray spectroscopy
TCP	Tricalcium phosphate
TH1	T helper type 1
TMI	Therapeutical metal ions
TNF α	Tumor necrosis factor-alpha
USA	United states of America
VEGF	Vascular endothelial growth factor
XRD	X-ray powder diffraction

1

INTRODUCTION

1.1 Bone

Bones have several essential roles in the body, including enabling movement, providing a framework for attachment of muscles and other tissues, protecting organs from injury, producing blood cells, maintaining calcium homeostasis, and buffering acids and bases. [1–3]

1.1.1 Anatomy and Physiology

The human skeleton consists of over 206 bones, varying in shape and size. These include long bones, such as those found in the limbs, as well as short bones such as those in the ankle and wrist, flat bones present in the skull, and irregular bones like the pelvis. [1,3] The extracellular matrix (ECM) of bone is composed of an organic, non-mineralized portion (primarily type-1 collagen) and an inorganic, mineralized portion, made of plate-like 4 nm thick carbonated apatite mineralites. Additionally, there are over 200 different non-collagenous matrix proteins (such as proteoglycans, glycoproteins, and sialoproteins) that contribute to the signaling within the bone's extracellular environment. The nanocomposite structure of bone, consisting of resilient collagen fibers reinforced with hydroxyapatite (HA) crystals, is crucial for its remarkable fracture toughness and compressive strength. [1–5] Bone tissue is organized into two types: cancellous (spongy) or cortical (compact) bone. The cancellous bone is less dense, highly porous, and arranged in plates, providing a high surface area-to-mass ratio, which enhances its role in ion exchange. It also offers structural support for the bone marrow it encases. Cortical bone, in contrast, is dense and composed of tightly packed osteons—cylindrical structures with a central canal containing a blood vessel surrounded by concentric layers of bone matrix. This type of bone encases the marrow cavity and provides mechanical strength. The outer surface of cortical bone is covered by the periosteum, a membrane rich in osteoblasts and blood vessels, which is activated during bone repair and appositional growth. Bone is a specialized, dynamic tissue that undergoes continuous remodeling in response to mechanical stress, adapting its architecture throughout life. [3–5]

1.1.2 Bone Formation

Bone formation occurs via two primary processes: endochondral and intramembranous ossification. Both mechanisms begin with the condensation of mesenchymal cells, which form a template for subsequent bone development. In intramembranous ossification, mesenchymal progenitor cells differentiate directly into osteoblasts, resulting in the formation of bones such as the mandible, clavicle, and various cranial bones. The majority of the bones in the body, including all long bones and vertebrae, are formed through endochondral ossification. In this process, mesenchymal progenitor cells first differentiate into chondrocytes, which generate a cartilaginous framework that is later mineralized and replaced by bone. Although there are differences in the composition and structure of bone between the two ossification pathways, both processes are regulated by similar molecular signals. [3,4]

1.1.3 Bone Damage Healing

Bone possesses a remarkable regenerative capacity, especially in younger individuals. [1,4] When a bone is fractured, the repair process mirrors aspects of both intramembranous and endochondral ossification, and it is notable for healing without scar tissue formation. Initially, a hematoma forms at the injury site, which triggers an inflammatory response and recruits various signaling molecules involved in bone regeneration, such as interleukins (ILs), tumor necrosis factor-alpha (TNF α), fibroblast growth factors (FGFs), bone morphogenetic proteins (BMPs), platelet-derived growth factor (PDGF), and vascular endothelial growth factor (VEGF). The repair and remodeling process begins within the periosteum, a layer rich in osteoprogenitors and osteocytes. These cells proliferate and migrate to the fracture site, forming a bony callus that facilitates healing. Most small fractures or bone defects heal naturally without the need for significant intervention. [1,3,4]

However, larger bone injuries are unable to regenerate on their own and often require surgical repair. The current gold standard for treating such injuries is autografting, wherein bone is harvested from a non-load-bearing region of the patient's body (commonly from the iliac crest) and transplanted to the site of the defect. Autologous bone grafting yields the best clinical outcomes, as it integrates well with the existing bone while avoiding immune rejection, which can occur with allogeneic (from human donors) or xenogeneic (from animals) bone grafts. [1,3,4]

Unfortunately, autografting is limited by the availability of donor bone and the morbidity associated with the harvest site. [1,3,4] This limitation has driven research into alternative bone regeneration methods, particularly in the field of tissue engineering. One approach involves the use of scaffolds that serve as a framework to guide the regeneration of new bone tissue. [1,3]

1.1.4 Bone Tissue Engineering

The classical framework for bone tissue engineering (BTE) emphasizes several key elements: a biocompatible scaffold that mimics the native bone ECM, osteogenic cells that generate bone tissue,

morphogenic signals that drive cellular differentiation into the desired phenotype, and sufficient vascularization to supply nutrients and remove waste. [1,3]

A major challenge in the field is achieving effective vascularization of tissue-engineered constructs, particularly for clinically relevant applications, and transitioning from animal models to human systems. Introducing controlled porosity within scaffolds may enhance permeability, promoting oxygen and nutrient diffusion, and facilitating the formation of a three-dimensional vascular network. Recent strategies for in-vitro "pre-vascularization" include the use of 3D multiculture systems that incorporate progenitor cells, mature differentiated cells, and endothelial cells, which are capable of forming organized vessel networks within the engineered tissue. The administration of angiogenic factors, such as vascular endothelial growth factor (VEGF), can also stimulate the growth of blood vessels. However, the use of potent biological agents like VEGF and growth factors that are involved in osteogenesis, such as the bone morphogenetic proteins (BMPs, eg., BMP2, and BMP7), has drawbacks. BMP administration is costly and can sometimes cause heterotopic ossification (bone formation in inappropriate locations). Efforts are underway to develop more refined delivery systems that address issues such as suboptimal release kinetics as well as the need for excessively high concentrations of GFs with short half-lives. Gene therapy offers another potential approach, allowing for localized and sustained expression of growth factors through genetically modified cells. However, the delivery vectors require optimization. Importantly, neither of these strategies fully replicates the complex and temporal sequence of GFs necessary for stable and stafe bone formation in vivo. [1]

1.2 Scaffolds and Biomaterials

Given the increasing clinical demand, the market for biomaterial-based treatments for bone repair is expanding rapidly. Bioactive materials work by interacting with biological molecules or cells to stimulate tissue regeneration. In bone repair, scaffolds need to exhibit specific properties to be effective, including osteoinductivity (the ability to promote the differentiation of progenitor cells into osteoblasts), osteoconductivity (supporting bone growth and encouraging the in-growth of adjacent bone), and the capacity for osseointegration (integrating with surrounding bone). Additionally, scaffolds must be rigid and resilient as they serve as the primary supporting three-dimensional framework for bone grafts, which facilitate the growth and regeneration of new bone tissue. They also need to be porous to promote nutrient, oxygen, and waste exchange while creating space for new tissue to form. Furthermore, they must be biocompatible to avoid triggering an immune response. [1,4] Scaffolds should replicate the natural extracellular matrix, enabling cell attachment and proliferation. Over the last two decades, numerous bone substitute materials have been explored as alternatives to autologous or allogeneic bone. These substitutes typically include bioactive ceramics, bioactive glasses, biological or synthetic polymers, or combinations of these materials. According to the principles of tissue engineering, the ideal scenario is for these materials to be gradually resorbed and replaced by newly regenerated biological tissue, as they

are intended to serve as temporary structures. [1] Scaffolds can be constructed from natural materials, synthetic materials, or composite materials composed of both.

1.2.1 Polymers

Various natural and synthetic polymers have been developed and recognized as biomaterials for bone tissue engineering (BTE). [3] Natural materials used in BTE include biological polymers such as collagen and hyaluronic acid, as well as inorganic materials like (HA) and β -tri-Calcium phosphate (β -TCP). The fibrous nature of polymers allows them to be easily manipulated during scaffold fabrication, granting precise control over the structure and porosity of the scaffold. [6,7] However, the presence of telopeptides within these polymers can sometimes provoke an immune response, and their inherent limitations—such as poor rigidity and rapid degradation—restrict their overall effectiveness in bone repair. [4]

Unlike natural materials, synthetic polymers can be designed and tailored to exhibit highly specific physical and chemical properties. Such properties enable control over the mechanical characteristics of scaffolds, such as tensile strength, durability, and degradation rate, while also achieving favorable biological outcomes, like minimizing risks of toxicity, immune reactions, and infection. [8] However, synthetic materials lack inherent bioactive properties like biocompatibility, osteoconductivity, and osteoinductivity, and therefore, must undergo additional modifications prior to use. [4]

The most commonly used synthetic materials for fabricating three-dimensional scaffolds are saturated poly- α -hydroxy esters, such as polylactic acid (PLA), polyglycolic acid (PGA), polylactic-co-glycolic acid (PLGA), and polycaprolactone (PCL). [8] These polymers can be processed through techniques like gas foaming, phase separation, salt leaching, fused deposition, and 3D printing. [9] The selection of polymers and fabrication methods for 3D scaffolds in tissue engineering has become a major field in material science, with significant advancements made over the past several decades. [10]

Recognizing that most materials have inherent limitations, researchers have begun designing and developing composite materials which combine polymers with inorganic minerals. This approach harnesses the complementary properties of different materials to optimize degradation rates and mechanical performance. The combinations and fabrication techniques for these composites are diverse and continually evolving. [11] Additionally, in engineered bone grafts, selecting materials that support vascularization is critical. Scaffolds with macroporous structures have been developed to promote vascular in-growth and incorporate vascular signals, such as growth factors or cells, beyond merely acting as osteoconductive platforms. [12]

Materials can influence the vascularization process in bone grafts through two main mechanisms: 1) by supporting the growth of endothelial cells and vessel formation, and 2) by incorporating active molecules that promote angiogenesis. For instance, 3D porous scaffolds made from silk fibroin and PCL have demonstrated strong support for endothelial cell growth and subsequent vascularization. [13,14]

Meanwhile, scaffolds made of PLGA and polylactide-co-glycolide (PLG) have shown to possess the ability to incorporate VEGFs and release them locally, enhancing the formation of new blood vessels. [15,16] Furthermore, the physical properties of scaffolds, such as porosity and geometry, can also impact their angiogenic potential. Research by Narayan, et al. demonstrated that pore size significantly affects endothelial cell growth, with smaller pores and reduced inter-pore distances promoting better cell proliferation. [17] The influence of the scaffold design on osteoconductive and vascular properties is still not fully understood and warrants further study. [18]

1.2.2 Polycaprolactone (PCL)

PCL is a relatively cheap and elastic synthetic aliphatic semi-crystalline polymer composed of hexanoate repeat units, that has been approved by the FDA, USA, and has been extensively used as a scaffold material in tissue engineering and regenerative medicine due to various desirable properties, such as excellent mix compatibility with many other materials, slow biodegradability, ease of processing, great mechanical stiffness and toughness at physiological temperature due to its low glass transition temperature and semi-crystalline nature. [19–24] Since It has slow and tuneable degradation, PCL has been blended with ceramic materials for specific applications, such as to improve its compressive or elastic modulus and tensile strength, since its inherent mechanical properties, although great compared to other polymers, still aren't on par with human tissues. [19–21,25] The hydrophobic nature of PCL inhibits cell adhesion and proliferation, which is why combining it with other osteogenic and osteoinductive compounds, such as hydroxyapatite and BG, or even growth factors, can improve its hydrophilicity and biocompatibility, to form better composite scaffolds for bone regeneration. [19,22]

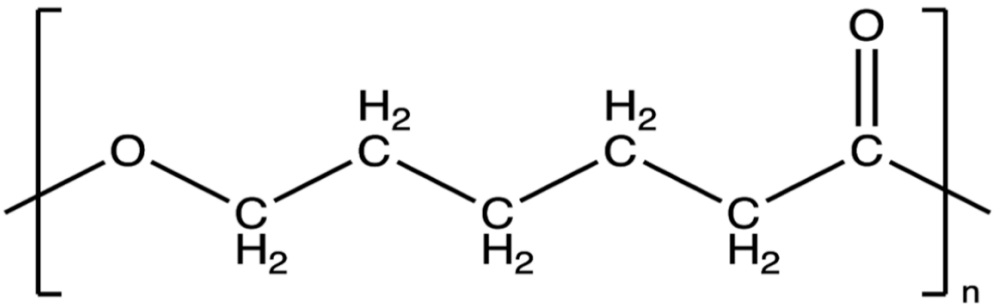

Figure 1. Chemical structure of polycaprolactone (PCL).

1.2.3 Bioglass

The first bioactive glasses were discovered by L.L. Hench in 1969, and they were termed 45S5 Bioglass®, with a composition by weight of 45% SiO_2, 24.5% Na_2O, 24.5% CaO, and 6% P_2O_5. Bioglasses are among the most bioactive materials due to their ability to form a hydroxyapatite layer, which shares a similar chemical composition and structure to that of bone minerals. [26] This layer forms as a result of rapid ion exchange between the bioactive glass and the surrounding physiological environment, allowing

for the migration of Ca^{2+} and PO_4^{3-} ions to the Bioglass surface, where they create an amorphous calcium phosphate layer that later crystallizes into hydroxyapatite. [27] Factors such as particle size, morphology, and crystallinity must still be carefully considered when designing hydroxyapatite-based biomaterials to enhance bone regeneration. [28]

This hydroxyapatite layer imparts Bioglass with valuable properties, such as osteoinductivity, osteointegrability, and angiogenesis, [29] by promoting the recruitment of stem cells and stimulating their differentiation into osteoblasts, thereby enhancing cell proliferation. Depending on the cell types used, concentration levels, and synthesis methods, Bioglass can also serve as a matrix for cell growth and development, promote blood vessel formation, and is non-toxic. [26,30,31]

1.2.4 Doped Bioglass

There is also the option of incorporating therapeutic metal ions (TMIs) into the composition of Bioglass, which can confer additional biological properties. These properties may include antibacterial activity, enhanced biological functionality, osteoconductivity, or improved mechanical characteristics. [32] TMIs can be added to the Bioglass network for their therapeutic effects and also to influence the glass structure and processability, as well as to provide extra-functional features like luminescence, fluorescence, radiation shielding, or anti-inflammatory properties. [33] Metallic ions are crucial for human health and could also be an alternative to expensive pharmaceuticals for imaging, diagnosis, and therapy. [34,35]

The presence of niobium (Nb) in biomaterials has been shown to improve their mechanical and bioactive properties. [36] Studies have shown that Nb ions promote osteogenic cell differentiation and mineralization. [37] The addition of niobium to ceramic matrices has demonstrated great corrosion resistance and low cytotoxicity. [29] For instance, Lopes et al. researched 45S5 Bioglass doped with 1%, 2.5%, and 5% molar concentrations of Nb_2O_5, prepared using a traditional melt-quenching method. The 2.5% and 5% concentrations exhibited delayed hydroxyapatite formation compared to undoped Bioglass and the 1% Nb_2O_5-doped sample. Cell studies confirmed the cytocompatibility, osteostimulation, and osteoinduction of Nb-doped Bioglass. In this study, Nb-doped glasses had no adverse effect on BMSCs. Moreover, osteogenic differentiation of BMSCs was induced at concentrations of 1 and 2.5 mol% Nb_2O_5 in 45S5 BG after 21 days using a glass concentration of 10 mg/mL. [38]

In a related study, Miguez-Pacheco et al. explored the in vitro behavior of bone marrow stromal cells (ST-2) exposed to extracts from 45S5 Bioglass containing varying concentrations of Nb_2O_5. Results indicated that high concentrations of 1 mg/mL were toxic to cells, while lower concentrations showed no adverse effects. When compared to undoped 45S5 BG, 0.5Nb content at 0.1 mg/mL showed a slight decrease in cell proliferation, while 1.0 Nb content presented a more pronounced decrease. At 0.01mg/mL, both 0.5Nb and 1.0Nb content showed a decrease in cell proliferation. Additionally, Nb-containing Bioglass demonstrated a significant release of VEGF at lower concentrations, suggesting a potential angiogenic effect. [39]

Characterization techniques like X-ray diffraction (XRD) and Fourier-transform infrared spectroscopy (FTIR) revealed that the addition of Nb did not alter the glass matrix. Raman spectroscopy also confirmed the presence of additional bands in the Nb-containing glass, associated with distortions in NbO_6 and vibration of NbO_4 units. The increase in NbO_4 units, compared to NbO_6, reduced bioactivity and antibacterial effects due to changes in the sample's electrical properties. [29]

1.3 Passivation

The process of passivation involves immersing Bioglass powder in distilled water or an incubation medium prior to scaffold production. This step is implemented to better simulate physiological conditions and to safeguard cells from the initial burst release of ions, which can cause a sharp increase in local pH levels. Such pH changes can lead to cytotoxicity and potentially obscure the accurate interpretation of cellular functions. [27,32,40,41] By limiting these pH variations, passivation allows for the formation of hydroxycarbonate apatite (HCA) to continue without disruption. [42] Research has demonstrated that this process enhances the in vivo capacity of the scaffold to support bone regeneration. [43] Various passivation protocols exist, differing in terms of duration and concentration. One particular study indicated that a 72-hour passivation protocol was equally effective as a 24-hour protocol, significantly reducing pH fluctuations in the culture medium and improving both cell viability and density compared to shorter protocols of 1, 6, and 12 hours. [40]

1.4 Enhancing Biofunctionality

To enhance the biofunctionality of scaffolds, integrating osteoinductive signals that attract the patient's endogenous stem cells post-implantation could eliminate the need for exogenous cell delivery and external growth factors. Achieving this goal requires creating biomimetic environments that replicate the natural cellular microenvironment. Cells are highly responsive to the physical cues in their surroundings, with surface topographies—such as grooves, ridges, and pits—at both the micron and nanoscale shown to influence cellular behavior. Research highlights that these topographic features can modulate processes ranging from cell adhesion to intracellular signaling pathways, thereby affecting transcriptional activity and gene expression. One study in bone tissue engineering examined the effects of random versus highly organized nanoscale surface features, revealing that mesenchymal stem cells (MSCs) are more inclined to differentiate and produce bone mineral when exposed to a certain degree of nanoscale disorder. The interaction between nanoscale surface topography, protein adhesion, and cellular behavior is complex, with outcomes depending on feature shape, size, and the specific proteins and cell types involved, necessitating further exploration. [1]

1.5 Macrophages

Macrophages are a type of white blood cell, more specifically, a type of myeloid cell and they are part of our innate immune system, in which they play a key role. [44]

1.5.1 Origin and Differentiation

These cells originate from monocytes circulating in the bloodstream and differentiate upon exposure to growth factors and cytokines present in the tissues they infiltrate. [45,46] Among their primary functions is cytokine production, whereby they release signaling proteins that modulate immune responses by recruiting other immune cells to sites of infection or inflammation. [47] Additionally, they are key players in phagocytosis, engulfing and digesting pathogens, cellular debris, and other harmful particles. [48] Following pathogen digestion, macrophages present antigens on their surface to T cells, an essential step in the activation of the adaptive immune response. [47] Beyond their immunological functions, macrophages contribute to tissue repair and wound healing by clearing apoptotic cells and promoting the regeneration of healthy tissue. [49,50]

1.5.2 Polarization

Macrophages are characterized based on their in vitro characteristics in cell culture. Macrophage polarization is referent to the state of activation of a macrophage at a certain point in time, but due to its plasticity, its polarization state is not fixed and can change based on the integration of signals from other cells, tissues, and pathogens. [51] Macrophage polarization is classified into two distinct phenotypes: the normally activated M1 macrophages and the alternatively activated M2 macrophages, which are differentiated based on their secretory profiles, functions, and surface receptor expression. [50] Recent studies have shown that macrophages typically exhibit a pro-inflammatory M1 secretory profile during the early stages of wound healing, and then they transition to an anti-inflammatory M2 gene expression profile during the later stages of wound healing. [52] M1 macrophages are associated with pro-inflammatory functions, including antigen presentation, the production of interleukins (IL-12, IL-23), and the activation of type-I T-cell responses. [47] They also release nitric oxide (NO) and other pro-inflammatory cytokines, which contribute to tissue damage and inhibition of cell proliferation. M1 macrophages are typically stimulated by interferon-gamma (IFN- γ), interleukin-1 β (IL-1 β), and lipopolysaccharide (LPS), driving strong immune responses against pathogens. [44,46,50]

Conversely, M2 macrophages are characterized by their anti-inflammatory and tissue-repairing roles. They exhibit limited antigen-presenting abilities, produce low levels of IL-12, and secrete high amounts of IL-10, IL-4, and IL-13, which contribute to their immunosuppressive effects. [47] M2 macrophages promote cell growth, tissue regeneration, angiogenesis, and clearance of cellular debris following

inflammation. They are also involved in activating type-2 helper T-cell responses (TH2) while suppressing type-1 responses (TH1). [44,46,47,50]

Although the M1 and M2 phenotypes are often viewed as distinct activation states, recent findings suggest that macrophages can exhibit features of both phenotypes depending on the context. For example, M2 macrophages may express some M1 markers, albeit at lower levels, and vice versa, highlighting the plasticity and complexity of macrophage polarization. [53]

2

MATERIALS AND METHODS

2.1 Synthesis of Bioglasses

The synthesis of the bioactive glass followed the Bioglass formulation established by Hench et al., comprising 45 wt% SiO_2, 24.5 wt% Na_2O, 24.5 wt% CaO, and 6 wt% P_2O_5. Additionally, 4 mol% Nb_2O_5 was introduced into the base Bioglass composition. The raw materials used included SiO_2 (Sigma-Aldrich, 99.8% purity), P_2O_5 (Sigma-Aldrich, 99% purity), $CaCO_3$ (Sigma-Aldrich, ≥99% purity), and Na_2CO_3 (PanReac Applichem, 99.5% purity). These were combined and thoroughly homogenized using a planetary ball mill (Fritsch Pulverisette 5) for 1 hour at 300 rpm, employing agate grinding jars and balls. The resulting mixture was subjected to calcination at 800°C for 8 hours. The glass was then melted via a quenching technique in a platinum crucible at 1300°C for 1 hour. To enhance homogeneity, the glass was re-melted under the same conditions. The obtained material was ground using an agate mortar to reduce the particle size, followed by additional milling in a planetary ball mill (Fritsch Pulverisette 7) for 1 hour at 300 rpm to achieve finer particles and a uniform size distribution.

2.2 Fabrication of Scaffolds

Composite scaffolds comprising PCL and Bioglass® were manufactured through solvent casting, hot pressing, and salt-leaching techniques. PCL (Sigma-Aldrich) was dissolved at an 8 wt% concentration in chloroform (Carlo Erba), to which 4 wt% NaCl particles (ranging from 100 to 200 µm) were added. Different composite mixtures were incorporated: 4 wt% non-passivated 45S5 BG (np 45S5BGs), 4 wt% passivated 45S5 BG (p 45S5BGs), 4 wt% non-passivated Nb4%-doped BG (np Nb4%s), and 4 wt% passivated Nb4%-doped BG (p Nb4%s). Each mixture was stirred vigorously on a magnetic stirrer overnight to ensure the formation of a homogeneous slurry. Films were cast from the solution, from which disks measuring 19 mm in diameter were cut. For each scaffold, three of these disks with salt layers between them were then hot-pressed using a platen press at 60°C under a pressure of 3 tons. Salt was leached out by soaking the samples in distilled water under continuous agitation for 30 minutes, followed by a

complete water replacement and additional immersion for 24 hours under constant agitation. Afterward, the samples were left on a Petri dish to dry for 48 hours.

2.3 Chemical Characterization

Small samples were cut from each scaffold type and the structural composition of them was analyzed using Fourier-transform infrared spectroscopy (FTIR). FTIR analysis was conducted using a Perkin-Elmer Spectrum BX FTIR™ spectrometer, scanning the range from 400 to 4000 cm^{-1}, a resolution of 4 cm^{-1} and also 128 co-added scans. During data acquisition, environmental conditions were controlled, maintaining room temperature at approximately 25°C and relative humidity at 37%.

2.4 Morphological Characterization

Small samples were cut from each scaffold type and the surface morphology of them was examined via scanning electron microscopy (SEM) using a TESCAN Vega 3 SEM. To enhance surface conductivity and reduce electron resistivity, the samples were coated with a thin layer of carbon before visualization. Particle size and distribution were quantified using ImageJ software, with 15 measurements taken per image for accuracy.

2.5 Cytotoxicity Assay (Saos-2 Cell Line)

The potential cytotoxicity of the prepared samples was assessed following the guidelines of ISO 10993-5, "Biological Evaluation of Medical Devices—Part 5: Tests for In Vitro Cytotoxicity," using the extract method and the Saos-2 human osteosarcoma cell line (ATCC® HTB-85™). For the BG powder cytotoxicity test, 200 mg of standard 45S5 BG and Nb4% BG were weighed and sterilized at 140°C for 4 hours. The extracts were prepared at a concentration of 100 mg/mL by incubating the bioactive glass powders in McCoy's 5A medium at 37°C for 24 hours. The solution was then centrifuged at 5000 G for 10 minutes, followed by filtration through a 0.22 µm Millipore filter, after which the extract was stored at 4°C. For passivated extracts, the bioactive glass powders were incubated for an additional 24 hours in fresh McCoy's 5A medium at 37°C, with the same subsequent processing steps.

For the scaffold cytotoxicity assay, two scaffolds of each type were selected, cut into 15mm in diameter disks, weighed, sterilized with 70% ethanol for 20 minutes, and air-dried in a laminar flow chamber for 24 hours. The scaffolds were rinsed with PBS and incubated in McCoy's 5A medium at 37°C for 24 hours. The medium volume was adjusted based on scaffold weight to achieve an extract concentration equivalent to 100 mg of BG per 1 mL of medium.

The Saos-2 cells were seeded at a density of 60,000 cells/cm^2 in 96-well plates and incubated at 37°C with 5% CO_2 for 24 hours. After removing the culture medium, the cells were exposed to the prepared

extracts. As a control, cells cultured in standard McCoy's 5A medium served as the negative control, while cells exposed to 10% dimethyl sulfoxide (DMSO) represented the positive control for cytotoxicity. After 48 hours of incubation with the extracts, a resazurin-based colorimetric viability assay was performed, with a resazurin-to-medium ratio of 1:1. The reaction proceeded for 3 hours, and absorbance readings at 571 nm and 601 nm were recorded using a UV-visible plate reader to assess cell viability.

2.6 Antibacterial Activity

With the goal of evaluating the antimicrobial properties of all samples, the agar diffusion method was employed using E.coli K12 DSM498 (DSMZ, Braunschweig, Germany) and S.aureus COL MRSA (methicillin-resistant strain which was provided by Rockefeller University). The bacterial strains were cultured overnight in tryptic soy broth (TSB) at 37°C in a humid atmosphere. The test samples, which were prepared as 7 mm diameter and ~2 mm thick disks, were sterilized by submerging in 70% alcohol for 20 minutes and then they were dried for 48 hours in a flow chamber. The two-layer bioassay was performed with TSB solidified using agar at 1.5% w/v for the base layer and 0.8% w/v for the top layer. Plates were prepared by pouring 20 mL of base layer and 4 mL of molten seeded overlay containing approximately 10^8 CFU/mL of the target microorganism. The test material disks were placed in specific locations on the plates, which were then incubated overnight at 37°C. Images of the resulting inhibition zones were taken.

Another assay was conducted, where 100 µl of a dilution of 1:10 of the original 10^8 CFU/mL of the microorganism in study was poured into a petri dish with solidified agar, then glass spheres were added and the petri dish was agitated in order to obtain a uniform distribution of bacteria. Then, the samples were added and photographs of the pellets were taken.

2.7 Adhesion and Proliferation (Saos-2 Cell Line)

In this assay, the scaffolds abillity to support cell adhesion and proliferation was examined. Scaffolds were cut into 15 mm in diameter disks, sterilized using 70% ethanol, and rinsed with PBS. The sterilized scaffolds and control materials were placed into 24-well plates and secured with silicone O-rings. Saos-2 cells were then seeded at a concentration of 20,000 cells/cm^2 directly onto the scaffold surfaces and at the bottom of the wells for the control group. The cells were cultured in McCoy's 5A medium and incubated at 37°C in a 5% CO_2 atmosphere for 24 hours. Cell adhesion was quantified using the resazurin reduction method, similar to the cytotoxicity assay. In this assay, the culture medium was replaced with a 1:1 mixture of resazurin and McCoy's medium, followed by a 3-hour incubation. The incubated medium was transferred to a 96-well plate, and absorbance at 571 nm and 601 nm was measured using a microplate reader (Biotek ELx 800 UV). To monitor cell proliferation, the resazurin assay was repeated at different timepoints, day 1, 3, 7, 10, and 14. Data from five independent biological experiments were

statistically analyzed, comparing both all samples at each time point and the performance of individual samples over time.

2.8 Alkaline Phosphatase (ALP) Activity (Saos-2 Cell Line)

Alkaline phosphatase (ALP), a well-established marker of osteogenic differentiation, [27] was measured using a colorimetric assay. The assay involved using 1 mg/mL of p-Nitrophenyl Phosphate (Sigma-Aldrich) dissolved in a tris-hydrochloric acid buffer. This experiment was performed after days 3, 7, 10, and 14 of the adhesion and proliferation tests. The process began by filtering the culture medium from the samples through a 0.22 µm Millipore filter, followed by measuring the absorbance at 405 nm to establish a baseline. The ALP solution was then added to the medium in a 1:1 ratio and incubated at 37°C for 20 minutes. After incubation, absorbance at 405 nm was measured again. Data from five independent biological assays were statistically analyzed, with comparisons made between samples at different time points and the same sample over multiple days. The population from the previous day was used for normalization.

2.9 Cytotoxicity Assay (THP-1 Cell Line)

Two samples ((a), and (b)) of PCL scaffolds, standard passivated 45S5BG, and Nb4%-doped BG were weighed, sterilized in 70% ethanol for 20 minutes, and then dried for 24 hours inside a laminar flow chamber. Then, they were washed with PBS and placed on a 12-well plate. In order to achieve the same concentration of medium to weight used as in the adhesion and proliferation assay with the 15mm disks, 802 µl of RPMI medium was added to each well (since the disks used in this assay are 19mm disks). After 24 hours, the medium was extracted from samples (a) of each scaffold and stored in an Eppendorf in the fridge at 5 ºC until the next step of the procedure, and then another 802 µl of the medium was added to each well of samples (a). This step was repeated two more times. After 72 hours, the medium was removed from samples (b) of each scaffold and replaced with new medium. After 24 hours the medium was extracted from samples (b) of each scaffold and stored in the fridge at 5 ºC. The THP-1 cell line was seeded at a concentration of 60kcell/cm^2 with 8 nM PMA in 96-well plates and incubated for 48h at 37◦C with 5% CO_2.

The culture medium was then replaced with the scaffold extracts. The negative control consisted of cells cultured in standard RPMI medium, while the positive control was cells exposed to a cytotoxic environment created by adding 10% DMSO.

After 48 hours of cell culture in the presence of the extracts, a colorimetric viability assay using resazurin was conducted. A 1:1 mixture of resazurin and medium was incubated with the cells for 3 hours. The absorbance at 571 nm and 601 nm was measured using a UV-visible plate reader to assess cell viability.

2.10 Macrophage Polarization (THP-1 Cell Line)

The THP-1 cell line was seeded at a concentration of 60 x 10^3 cell/cm^2 with 5 µl of PMA per 10mL of medium, in 24-well plates and incubated for 48h at 37ºC with 5% CO_2. Three controls were used, one with PMA, in order to study the M0 phase of the monocytes, one with 100 ng/mL of LPS and 20 ng/mL of INF-y, in order to induce M1 phase differentiation of the macrophages, and then one with 20 ng/mL of IL-4 and 20 ng/mL of IL-13, in order to induce M2 phase differentiation of the macrophages. Timepoints were taken at 24, 48, and 72 hours of each sample and control. This was done by removing the medium, washing with PBS, then adding 4% paraformaldehyde (PFA) for 20 minutes, then removing the PFA and washing with PBS, transferring to another 24-well plate, and leaving each sample and control in PBS until the immunofluorescence assay.

The immunofluorescence assay was realized by washing each sample with PBS, then adding 400 µL of 0.3% Triton-X100 for 15 min per well, washing with PBS, and adding 400 µL of 2% BSA in PBS for 1 hour. Then washing with PBS and placing the samples and the controls on top of a parafilm sheet over a pipette tip box filled with water. Primary antibodies were prepared in a concentration of iNOS 1:500, and CD163 1:500, in a solution of 0.3% Triton-X100 + 1% BSA in PBS. Then, 100 µL of primary antibodies were added to each sample and 50 µL of the same primary antibodies were added to each control and the box was stored at 4°C overnight, covered with an aluminum sheet in the dark.

The next day, the samples and controls were washed with PBS and the secondary antibodies were prepared at a concentration of 1:1000 in 1%BSA. 100 µL of the antibodies were added to each sample and 50 µL to each control, then they incubated at room temperature, in a dark room for 90 minutes. Then, each sample and control was washed with PBS and 100 µL of 10 µM DAPI solution in PBS was added to each scaffold, whilst 50 µL of the solution was added to each control for 5 minutes. Then each sample and control was washed with PBS and distilled water. Then, the samples were mounted in 20 µL of Mowiol, whereas the controls were mounted in 10 µL of Mowiol, and they were let dry overnight at room temperature in a dark room. Then, when the Mowiol was completely dry, all of the samples and controls were stored in the fridge at 4 ºC until observation. iNOS is a hallmark M1 macrophage marker, whilst CD163 is a M2 macrophage marker. The red marker was used for the iNOS antibodies, whilst the green marker was used for CD163.

3

RESULTS & DISCUSSION

3.1 SEM

With the goal of evaluating the scaffold's ability to provide a fit environment for cell growth and proliferation, the samples were analyzed by SEM-EDS. In Figure 2, it is possible to observe that the scaffolds that contained bioglass have slightly higher pore size, much higher pore density, and interconnectivity than the PCL scaffolds, probably due to the fact that the scaffolds have less concentration of PCL. The importance of having pore interconnectivity is high, due to the fact that it is what matters most in terms of achieving vascularization in the tissue in which the scaffold is implanted, which is crucial for the enchondral and intra-membranous ossification process, as well as in consequent bone remodeling and formation processes, given its importance in supplying nutrients and oxygen to the active bone tissue and consequent removal of waste products. [54] Nevertheless, all scaffolds present a porous network In their Internal structure, which Is suitable for cell Infiltration, and thus, provides a more suitable environment for cell growth. In Table 1 we can see the average pore size for each type of scaffold, which is around 116 µm for the PCL scaffolds, and around 140 µm for both the standard bioglass scaffolds and the niobium-doped bioglass scaffolds. This is consistent with a suitable environment for cell growth. Since SEM Images were only collected for one batch of each scaffold, the sample size of the scaffolds Is small, since batches can vary among them, and SEM Images of the scaffolds immersed in SBF throughout several time points could have been taken in order to study the formation of a layer of Ca/P, which is a composition that could possibly be used as an osteoconductive material in bone repair and regeneration, thus a larger sample size of SEM Images for each scaffold and in several conditions could allow for a better characterization of the topography of the surface of the scaffolds, its Internal structure and its bioactive properties. With this In mind, future investigations should account for this limitation, eliminating it for more consistent and reliable results.

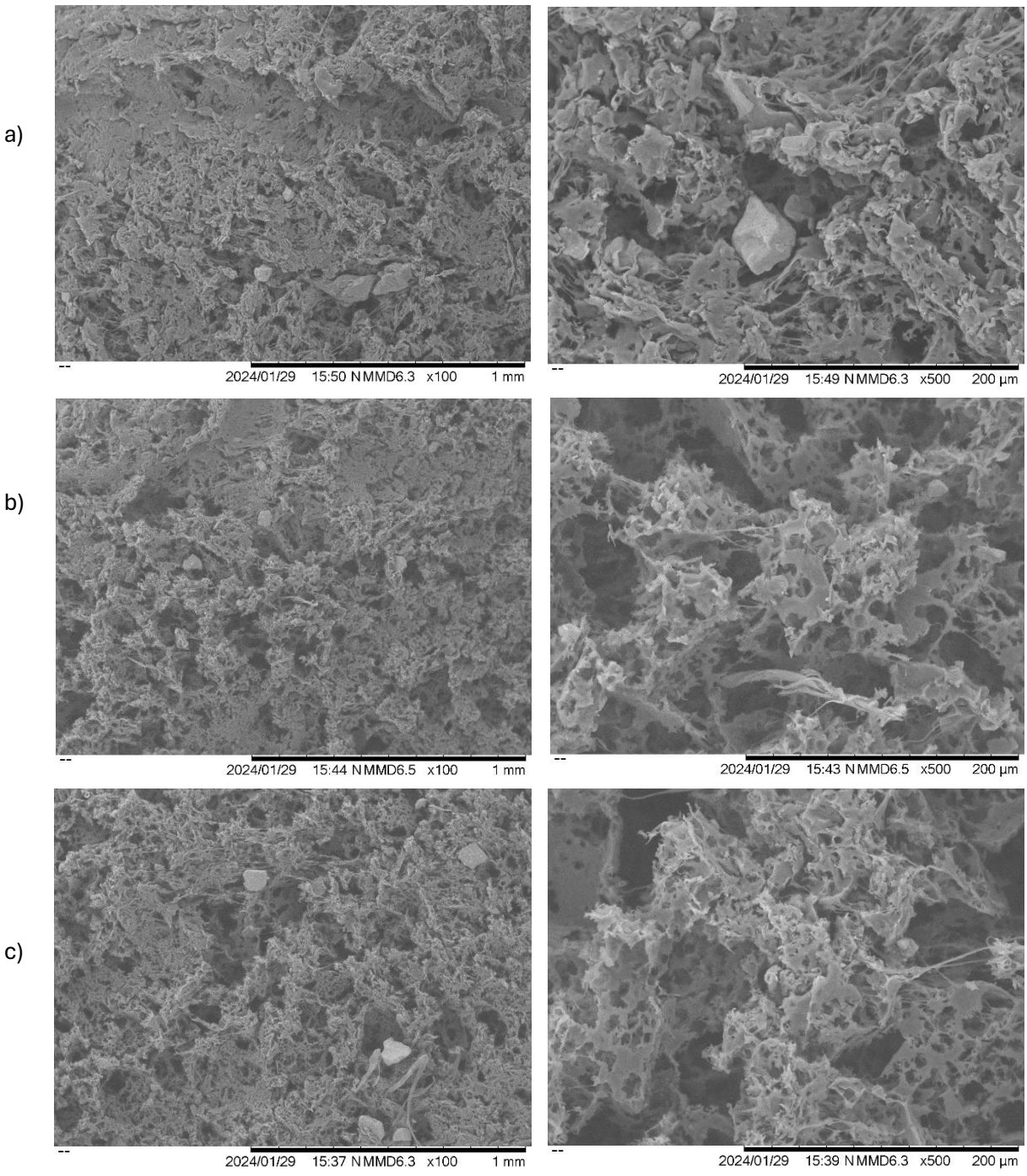

Figure 2. SEM images of the surface of the PCLs (a) 45S5BGs (b) and Nb4%BGs (c).

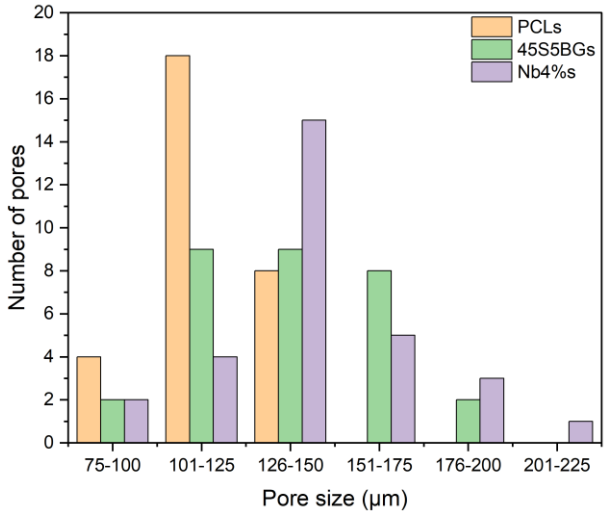

Figure 3. Pore size distribution per sample of PCL and composite membranes.

Table 1. Average scaffold pore size (µm).

Sample	Pore Size (µm)
PCL	116 ± 16
BASE	141 ± 22
NB4%	143 ± 28

3.2 FTIR

The FTIR spectra for PCLs, 45S5BGs, and Nb4%BGs are shown in Figure 4. Based on the images, the inclusion of niobium into the 45S5 Bioglass network does not influence the typical vibrational bonds. The characteristic vibration bands of this type of bioactive glass can be seen in the spectrum. The peaks around 1045 cm^{-1} and 933 cm^{-1} correspond to the asymmetric stretching of Si-O-Si, while the band at approximately 732 cm^{-1} represents the symmetric stretching of Si-O-Si. Additionally, the band at 524 cm^{-1} is linked to the bending mode of Si-O-Si bonds. The shoulder near 586 cm^{-1} is attributed to the P-O bending mode from the amorphous phosphate, a feature commonly seen in 45S5 Bioglass. [43,55–58] Consequently, it can be inferred that the introduction of niobium into the bioglass structure does not result in any significant alterations to the glass matrix.

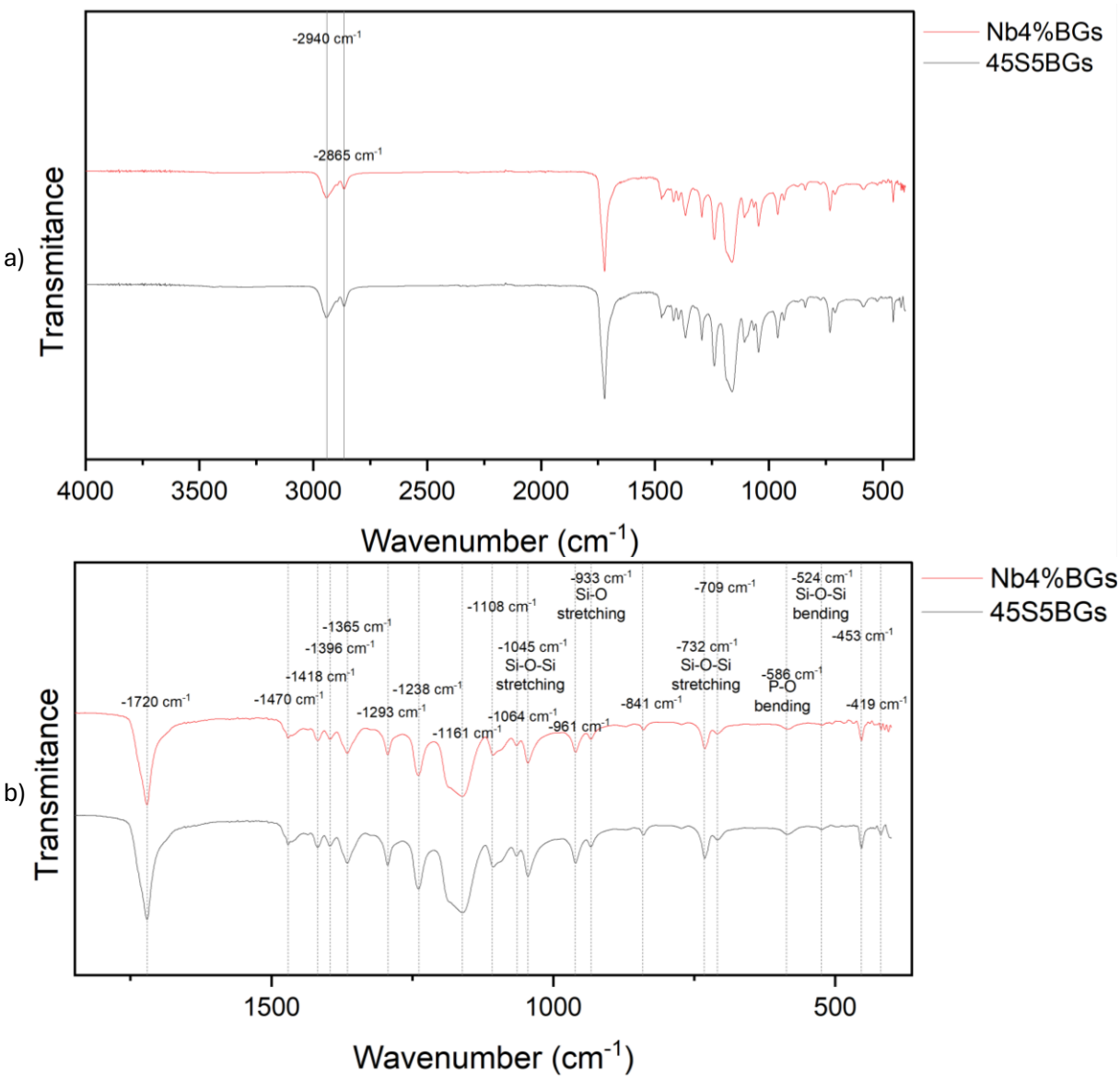

Figure 4. (a) 4000-400 cm^{-1} and (b) 1800-400 cm^{-1} FTIR spectra of 45S5BGs and Nb4%BGs, with the relevant vibrations identified and matching wavenumber.

3.3 Saos-2 Cytotoxicity

The goal in this part of the experiments is to determine which of the samples produced have higher cell survivability and at which concentration they exhibit better performance.

3.3.1 BG Powder Cytotoxicity Assay

Figure 5.a) presents the results from the base powder extract cytotoxicity assay with the Saos-2 cell line. It shows that by passivating the bioglass powder we can achieve higher cell viability than by not submitting the powder to this process. This is due to the fact that, when put in contact with water or any medium for the first time, the bioglass will burst release ions, which results in an extreme increase in pH, leading to pH-dependent cytotoxicity. [40,59–62] Some concentrations of bioglass achieved higher cell

viability than the control group, confirming that the introduction of bioglass in culture medium provides a more adequate environment for cell proliferation.

Figure 5.b) presents the results from the niobium-doped powder extract cytotoxicity assay with the Saos-2 cell line. These results are in accordance with the data from Figure 1, seeing as the passivated powder attained higher cell viability, supporting the idea that passivating the powder should be the standard, with the purpose of achieving the highest possible cell viability. It also shows that niobium-doped BG ensures higher cell survivability than standard BG. Niobium-doped bioglass also provides a better environment for cell proliferation than standard McCoy medium, as evidenced by the results obtained. This is probably due to the fact that the presence of niobium ions promotes cell growth and provides a low cytotoxic environment. [29]

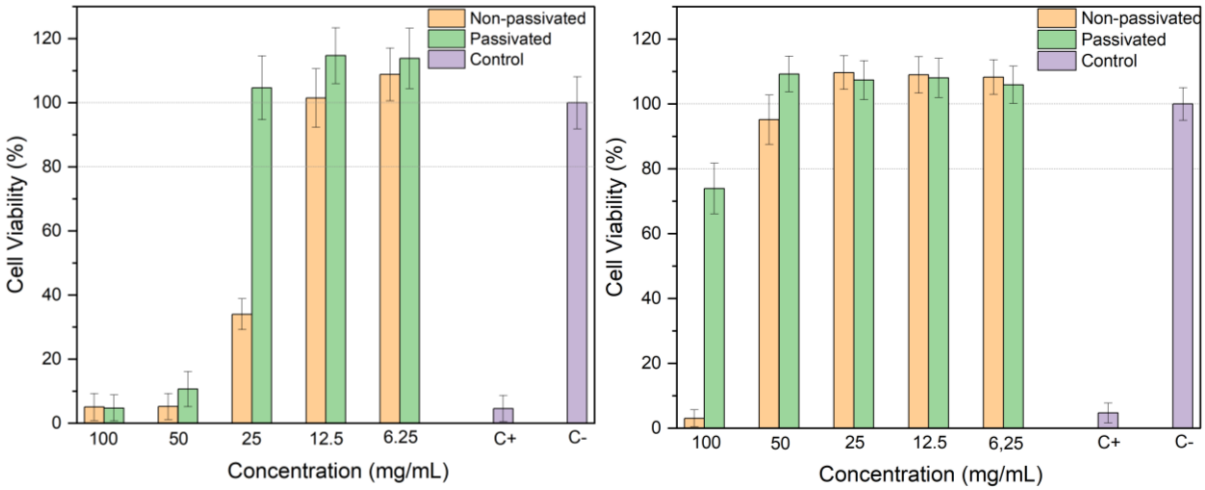

a) b)

Figure 5. Cytotoxicity assay results of (a) 45S5BG and (b) Nb4%BG (Nb4) powder.

3.3.2 Scaffold Cytotoxicity Assay

Figure 6 presents the results from the PCLs cytotoxicity assay with the Saos-2 cell line. These results show that the PCLs are biocompatible with Saos-2, as was expected since this biomaterial has been extensively researched and is regarded as one of the safest and most used polymers in tissue engineering. [19–25]

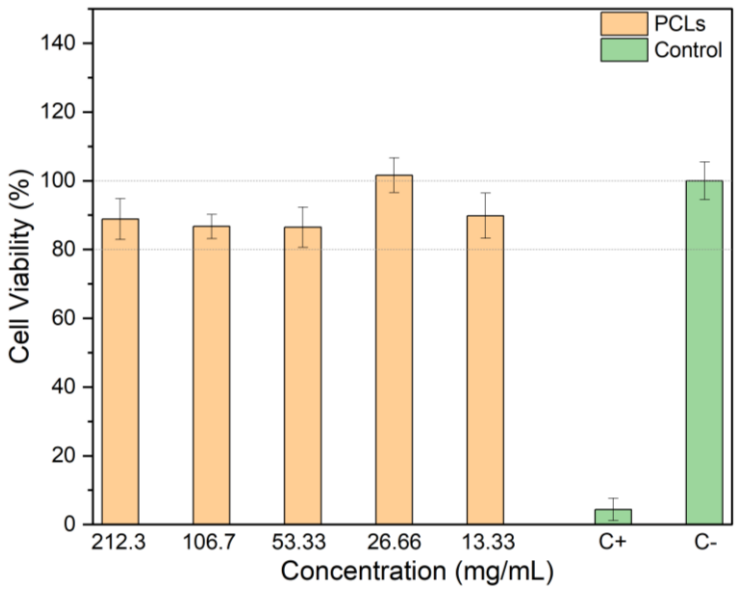

Figure 6. PCLs cytotoxicity assay results.

Figure 7.a) presents the results from the non-passivated scaffold cytotoxicity assays. Through observation of this data, it is possible to conclude that the Nb4%BGs ensure higher cell survivability and proliferation than the 45S5BGs , which is in agreement with the results from Figures 1 and 2. This assay also shows that niobium-doped BG scaffolds attained higher cell proliferation than the McCoy medium control group, which shows the potential that Nb-doped BG has in regards to enhancing cell proliferation. Figure 7.b) presents the results from the passivated scaffold cytotoxicity assays. These results are in accordance with the literature and with what was stated earlier in regards to passivation granting higher cell survivability than not passivating the samples. Once again, it also shows that Nb-doped BG provides a better environment for cell proliferation and survival than standard 45S5BG. The likely explanation for this is that the presence of Nb ions accelerates the release of Na+ ions, which are exchanged with H+ and H3O+ ions from the surrounding medium. This exchange raises the pH of the solution as cations replace the sodium ions, facilitating the breakdown of the Si-O-Si bonds. As a result, the glass dissolves more quickly, which leads to the formation of silanol groups that accumulate on the glass surface. These silanol groups then condense to form a hydrated silica layer that promotes the nucleation of carbonated hydroxyapatite. [29,63,64] This hydroxyapatite layer enhances bioactivity, biocompatibility, and the mineralization and differentiation of osteogenic cells. [37,65]

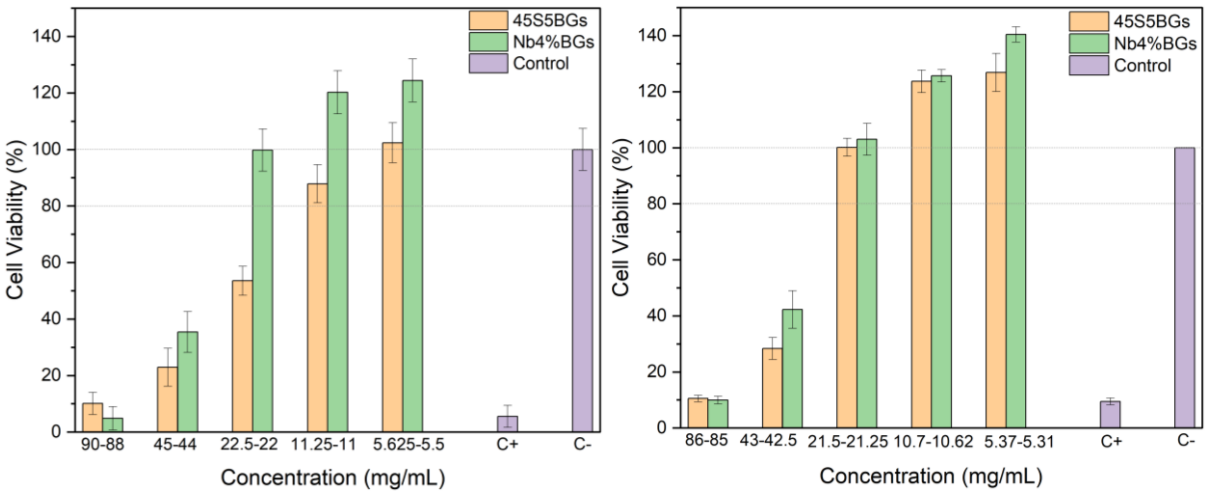

a) b)

Figure 7. Cytotoxicity assay results of (a) non-passivated scaffolds and (b) passivated scaffolds.

3.4 Anti-bacterial Activity

In Figure 8. it is possible to confirm that there was no apparent anti-bacterial activity. This is an unexpected result since BG scaffolds have been shown to possess some antibacterial effects. The more likely causes of this are that since the control medium was later confirmed to be contaminated, there might have been too high of a bacteria concentration in the Petri dishes, or there might even be cross-contamination of other bacterial species. Another possibility is that there weren't enough ions diffused from the scaffolds onto the plaques, which might be explained by a lack of permeability. This lack of ions diffused might also be explained by a lack of enough BG present in each sample.

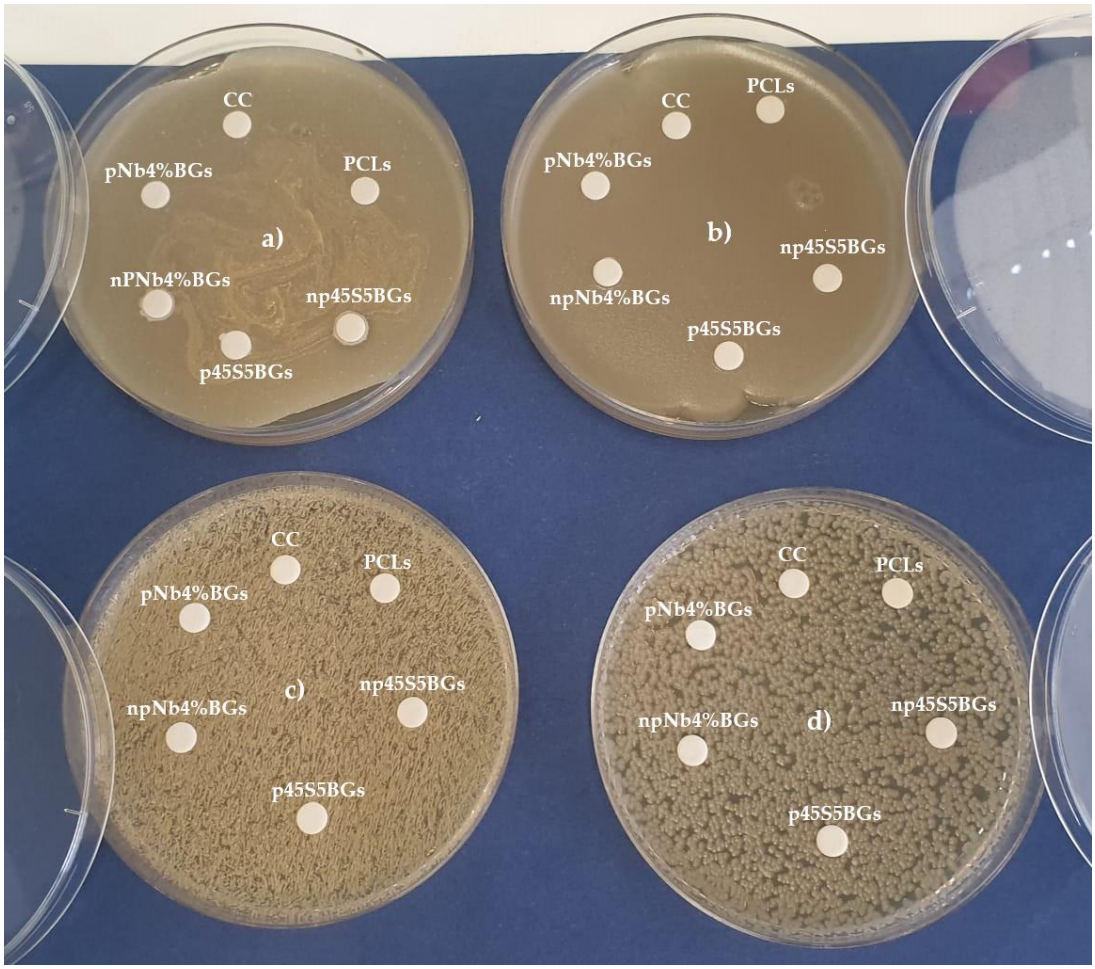

Figure 8. Two-layer bioassay with E.coli (a) and S.Aureus (b) and glass sphere bioassay with E.coli © and S.Aureus (d) anti-bacterial activity results.

3.5 Saos-2 Adhesion and Proliferation

An assay was performed over the course of 10 days, with five different replicates for each sample, with the goal of inferring about the scaffold's ability to promote cell adhesion and proliferation.

After 24 hours of the cells being seeded, the first evaluation was conducted through a resazurin assay, which established the first day of viability, and thus, the standard for cell growth (100% mark). Then, further measurements were taken for 14 days. Through the material control, resazurin control, and first-day viability control, it was possible to calculate the cell adhesion and proliferation over the expected course of the experiment. The results obtained are displayed in Figure 9. The PCLs showed the highest rate of adhesion and proliferation of all the samples, presenting an increase in population throughout the course of the whole experiment, followed by the Nb4%BGs, with these samples increasing in population throughout days 1 to 10 and then decreasing slightly between days 10 and 14. Meanwhile, the 45S5BGs appear to negatively affect the adhesion and proliferation of cells, since the results obtained are of nearly 0% population throughout the whole experiment.

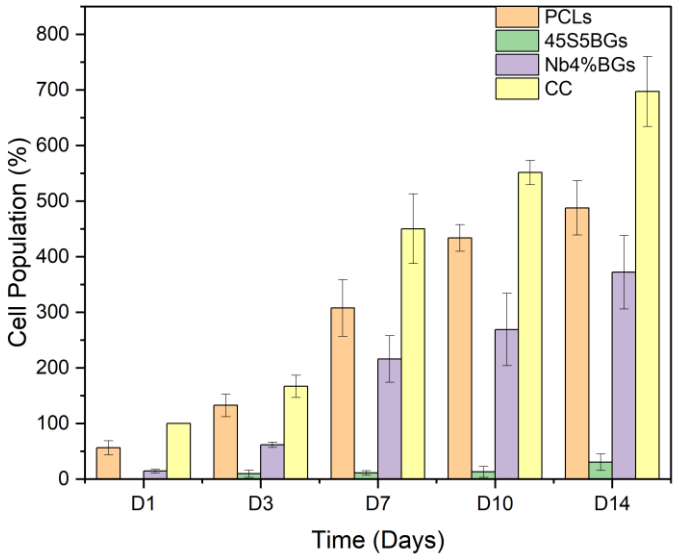

Figure 9. Cell adhesion and proliferation assay results from Saos-2 cells seeded in the different scaffolds. After seeding, measurements were taken on days 1, 3, 7, 10 and 14. The data obtained results from five biological replicates and statistics.

Table 2. Proliferation rate of each sample.

Sample	Proliferation Rate (D14/D1)
PCLs	8.6 ± 3.8
45S5BGs	50.83 ± 27
Nb4%BGs	25.96 ± 8.6
CC	6.97 ± 0.63

3.6 Saos-2 ALP

Through the analysis of ALP production in Figure 10., it is possible to observe that the Nb4%BGs present higher ALP production, almost as high as the cell control during days 4, 8, and 11. This is indicative of the fact that the niobium ions promote cell viability and increase ALP activity, as has been reported in other studies. [66–68] In contrast to these results, the 45S5BGs have shown to be a hindrance to the production of ALP, which may be related to the low proliferation of the Base BG scaffold throughout every day of the assay, and throughout every biological replicate. Another study has reported similar results to those of the 45S5BGs. [27] The PCLs results show that despite being a reliable material, PCL alone is not enough to induce the level of ALP production that is wanted, which is why it is a material that should be combined with other materials, that can enhance its properties to desirable levels. [19–22,25]

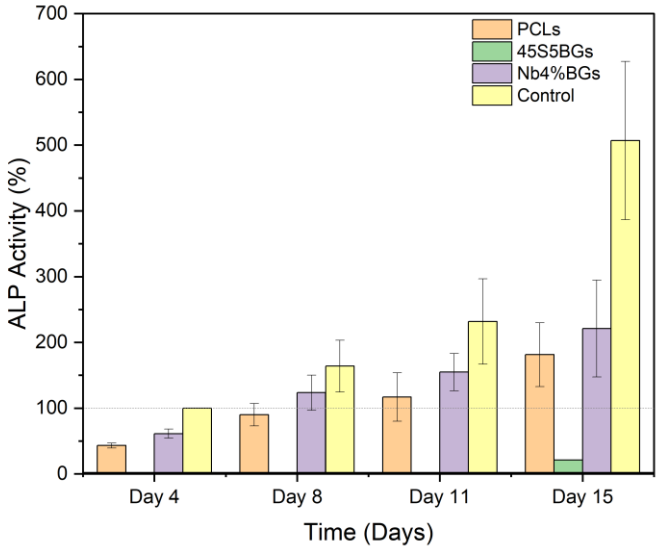

Figure 10. ALP assay results from Saos-2 cells seeded in the different scaffolds. After seeding, measurements were taken on days 4, 8, 11 and 15. The data obtained results from five biological replicates and statistics.

3.7 THP-1 Cytotoxicity

Figure 11 presents the results from the THP-1 cell line cytotoxicity assay. It is possible to confirm that the scaffolds are not cytotoxic to the THP-1 cell line, with the exception of the 96-hour sample of the 45S5BGs. These results show that it is possible to seed the cells into the samples without any prior passivation using RPMI medium, seeing as both 24-hour samples achieved higher than 80% cell viability. Additionally, all NB4%-doped BG samples present results that show that they improve cell growth and viability, seeing as they have higher cell viability than the negative control group (live cells with RPMI) making it a promising candidate for a macrophage growth-enhancing material.

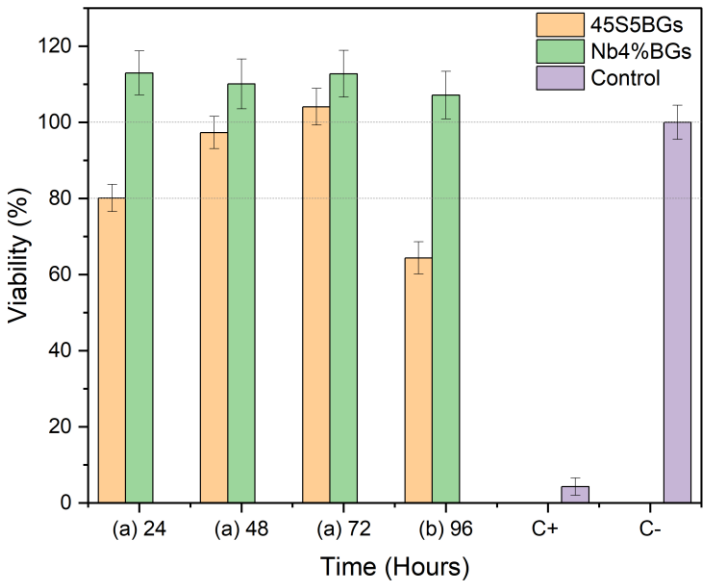

Figure 11. Passivated 45S5BGs and Nb4%BGs THP-1 cytotoxicity assay results.

3.8 THP-1 Immunofluorescence

As mentioned before, iNOS is a hallmark M1 macrophage marker, whilst CD163 is a M2 macrophage marker. The red marker was used for the iNOS antibodies, whilst the green marker was used for CD163. The blue stained dots in the blue filtered image represent the nucleus of the cells.

In Figures 12, 13 and 14. there appears to be an abundance of cells throughout the 3 days, in all of the filtered images, with the red-filtered image appearing to have more cells than the green-filtered images. These images show that there was indeed growth of cells, without much polarization, other than the natural one.

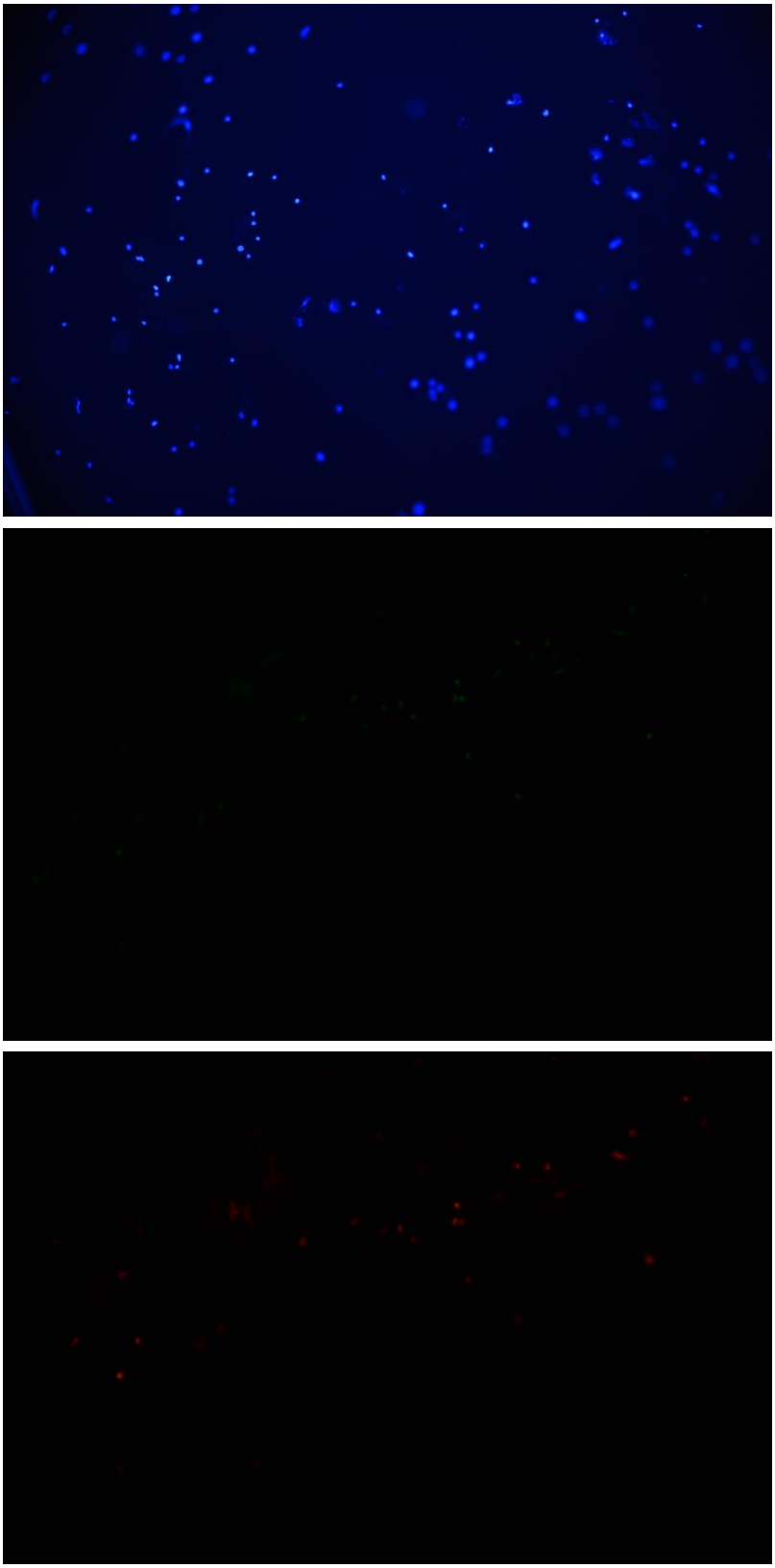

Figure 12. Immunostaining images of M0 control group at 24 hours of macrophage polarization at x100 zoom.

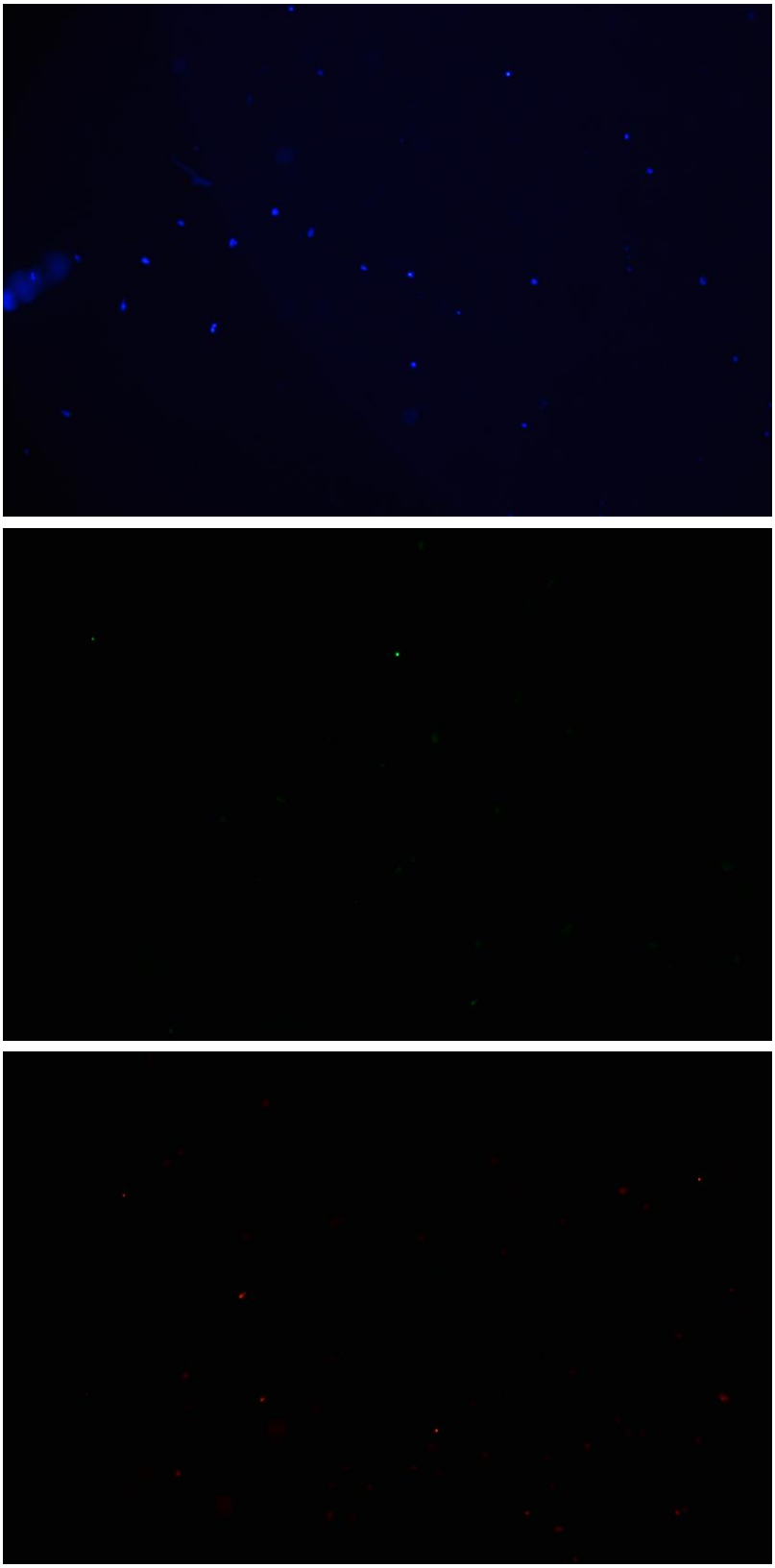

Figure 13. Immunostaining images of M0 control group at 48 hours of macrophage polarization at x100 zoom.

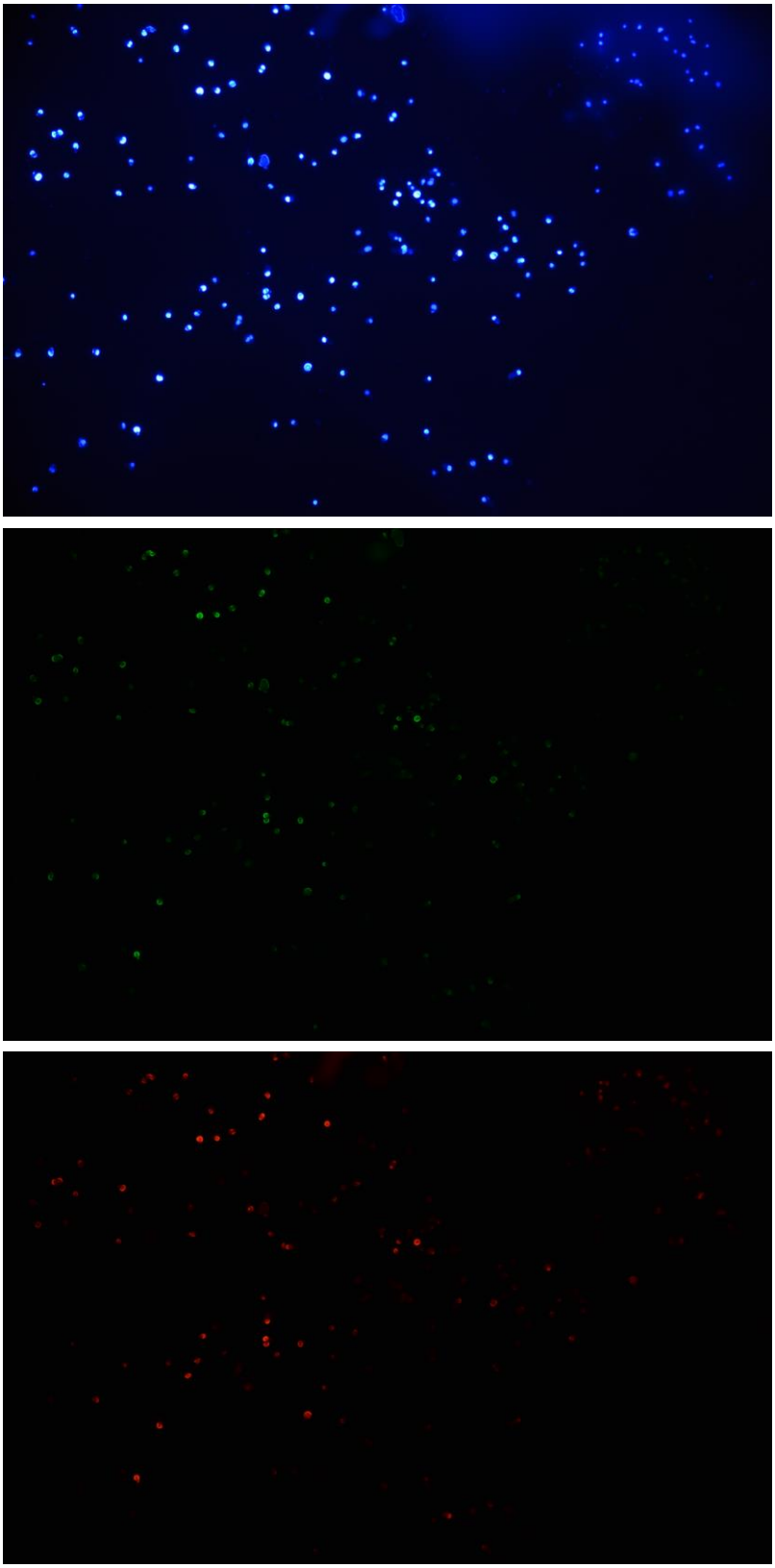

Figure 14. Immunostaining images of M0 control group at 72 hours of macrophage polarization at x100 zoom.

In Figures 15, 16 and 17. there is once again a great abundance of cells throughout all of the Images, with the red-filtered image appearing to have more cells than green-filtered image. As it can be observed, with the red-filtered having many more cells, a successful M1 control group was achieved.

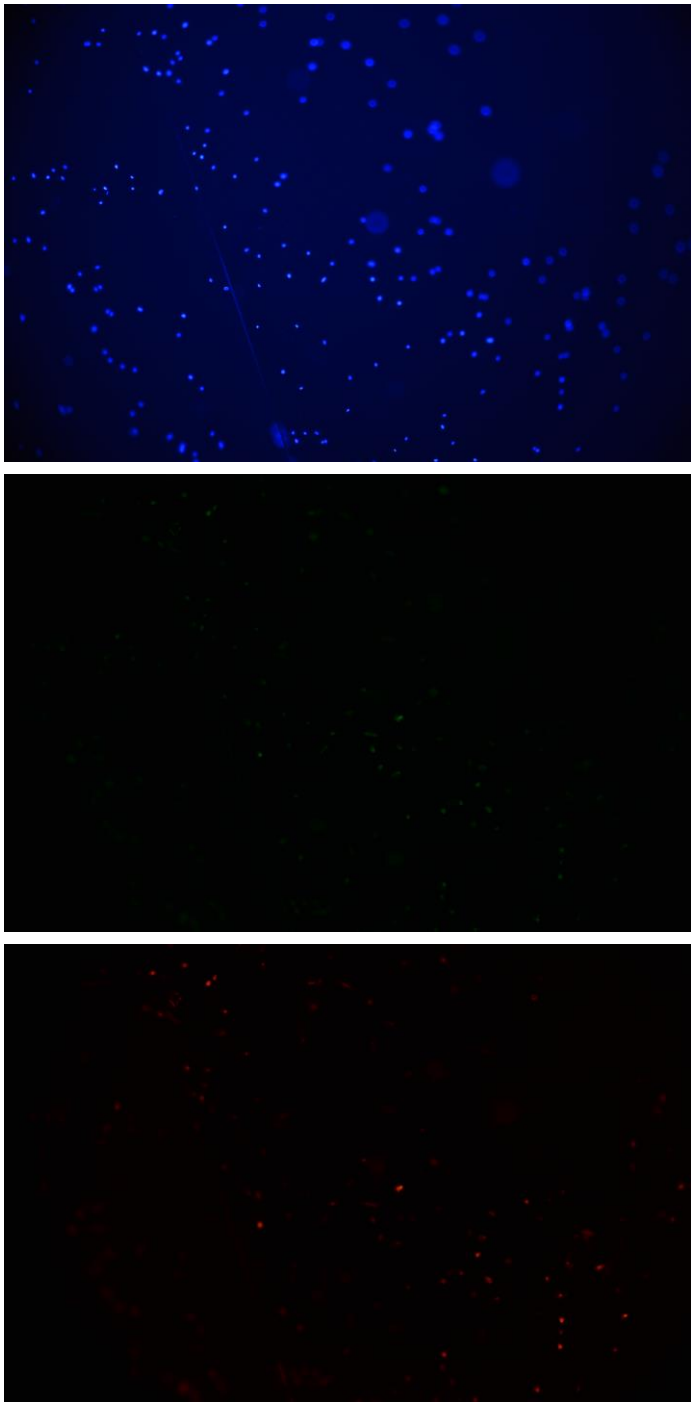

Figure 15. Immunostaining images of M1 control group at 24 hours of macrophage polarization at x100 zoom.

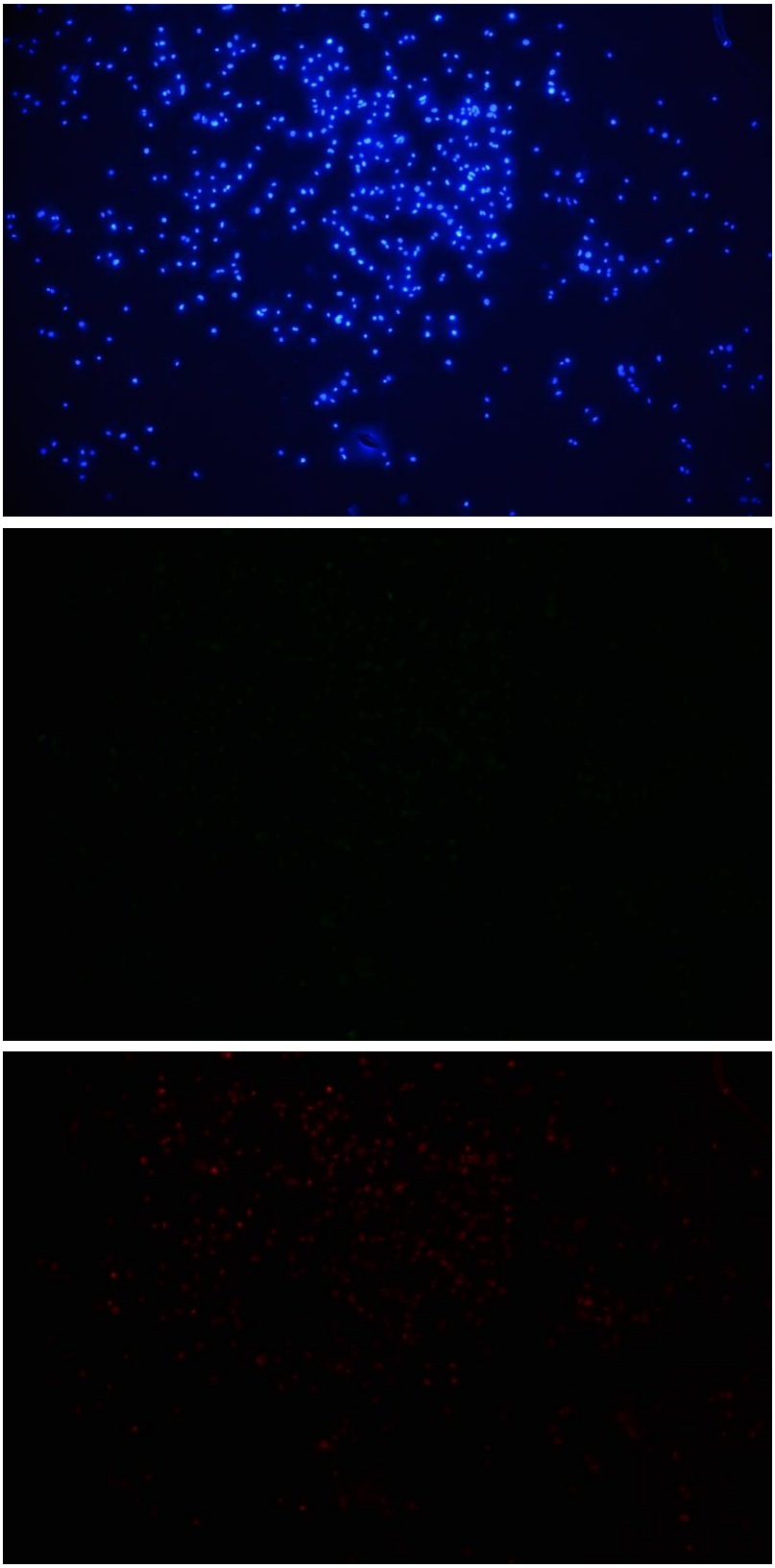

Figure 16. Immunostaining images of M1 control group at 48 hours of macrophage polarization at x100 zoom.

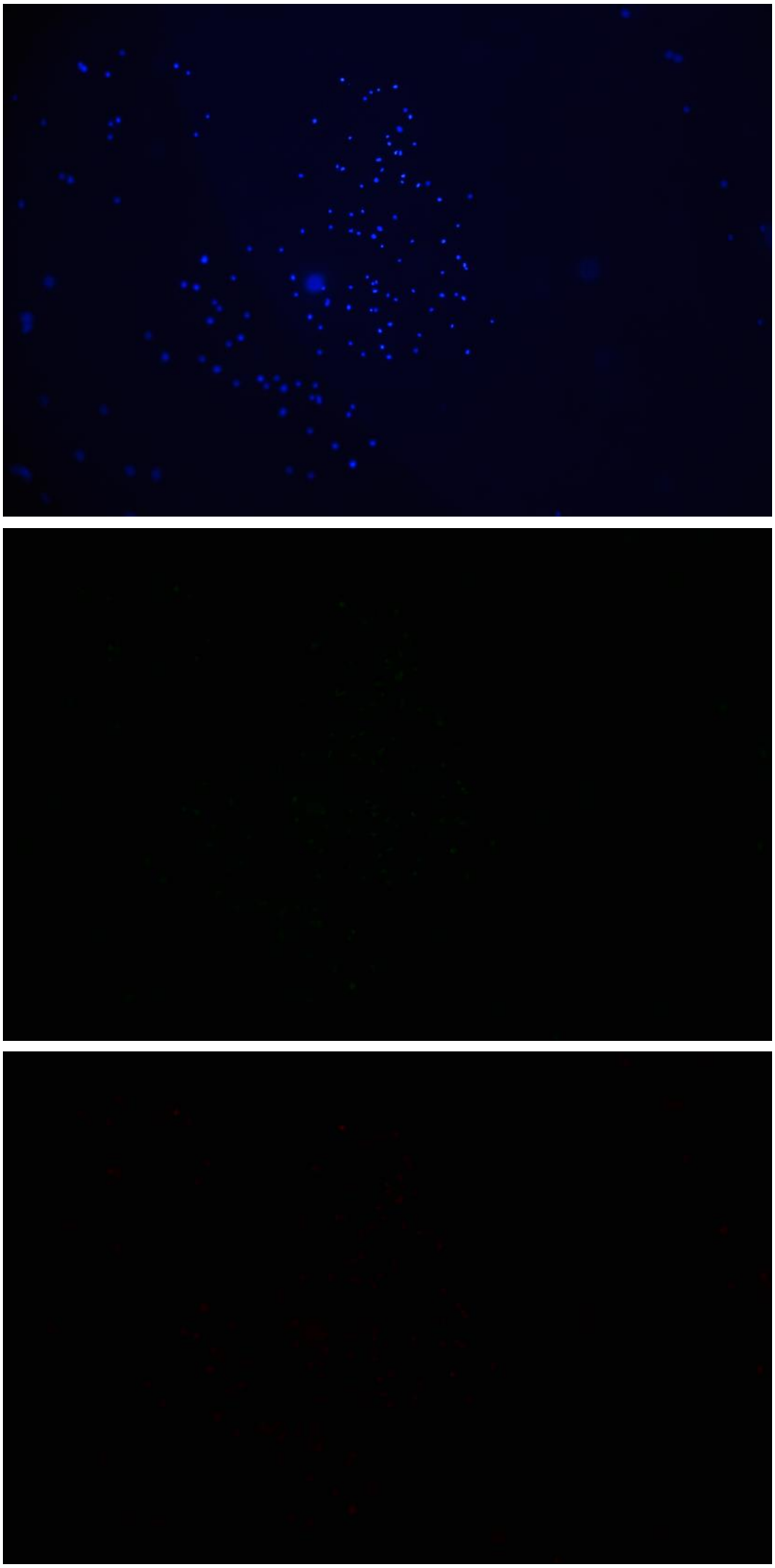

Figure 17. Immunostaining images of M1 control group at 72 hours of macrophage polarization at x100 zoom.

In Figures 18, 19 and 20. there seems to be less abundance of cells compared to the M0 and M1 control groups, with day 3 presenting the most amount of cells and the red-filtered image having more visible cells than the green-filtered image. Contrary to the previous control groups, this one presents much less cells, and a successful M2 control groups wasn't achieved, seeing as there aren't many green dyed cells.

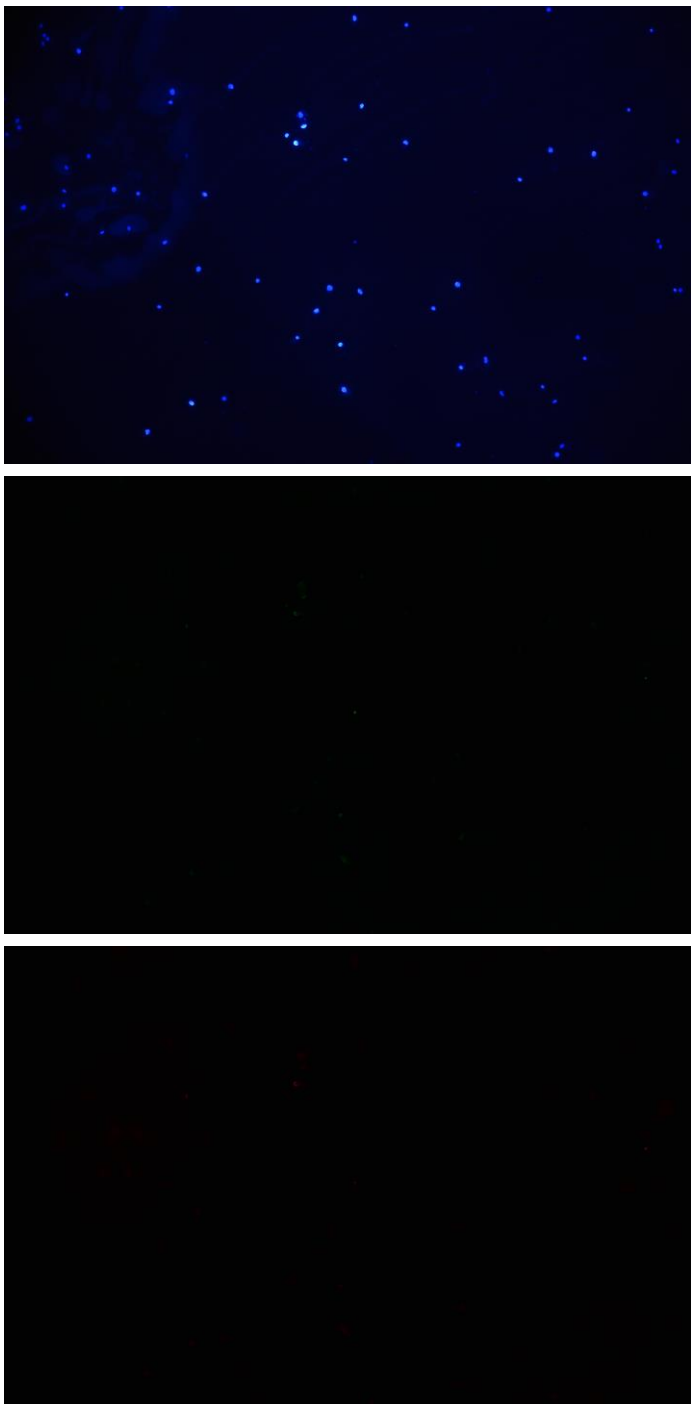

Figure 18. Immunostaining images of M2 control group at 24 hours of macrophage polarization at x100 zoom.

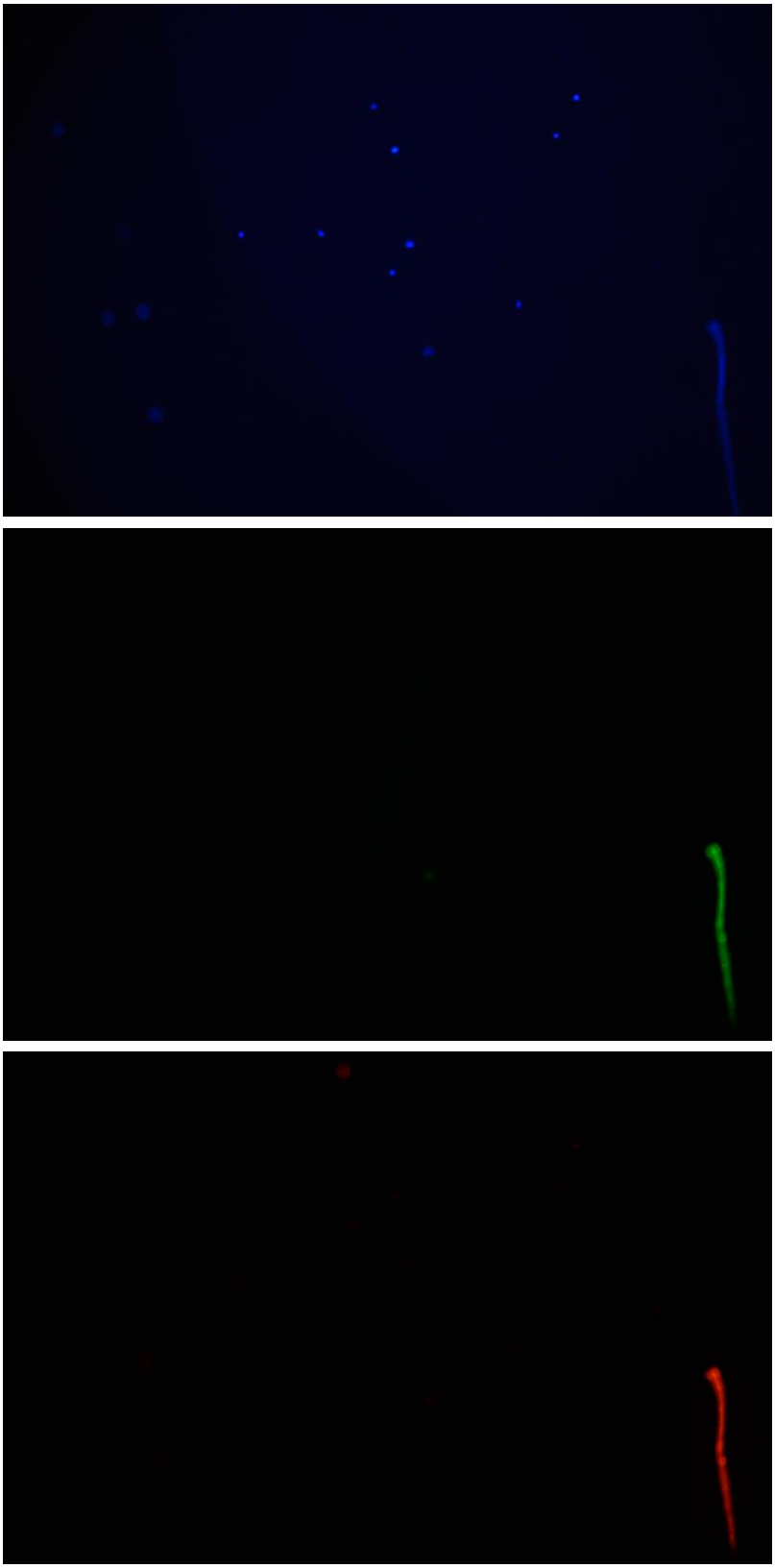

Figure 19. Immunostaining images of M2 control group at 48 hours of macrophage polarization at x100 zoom.

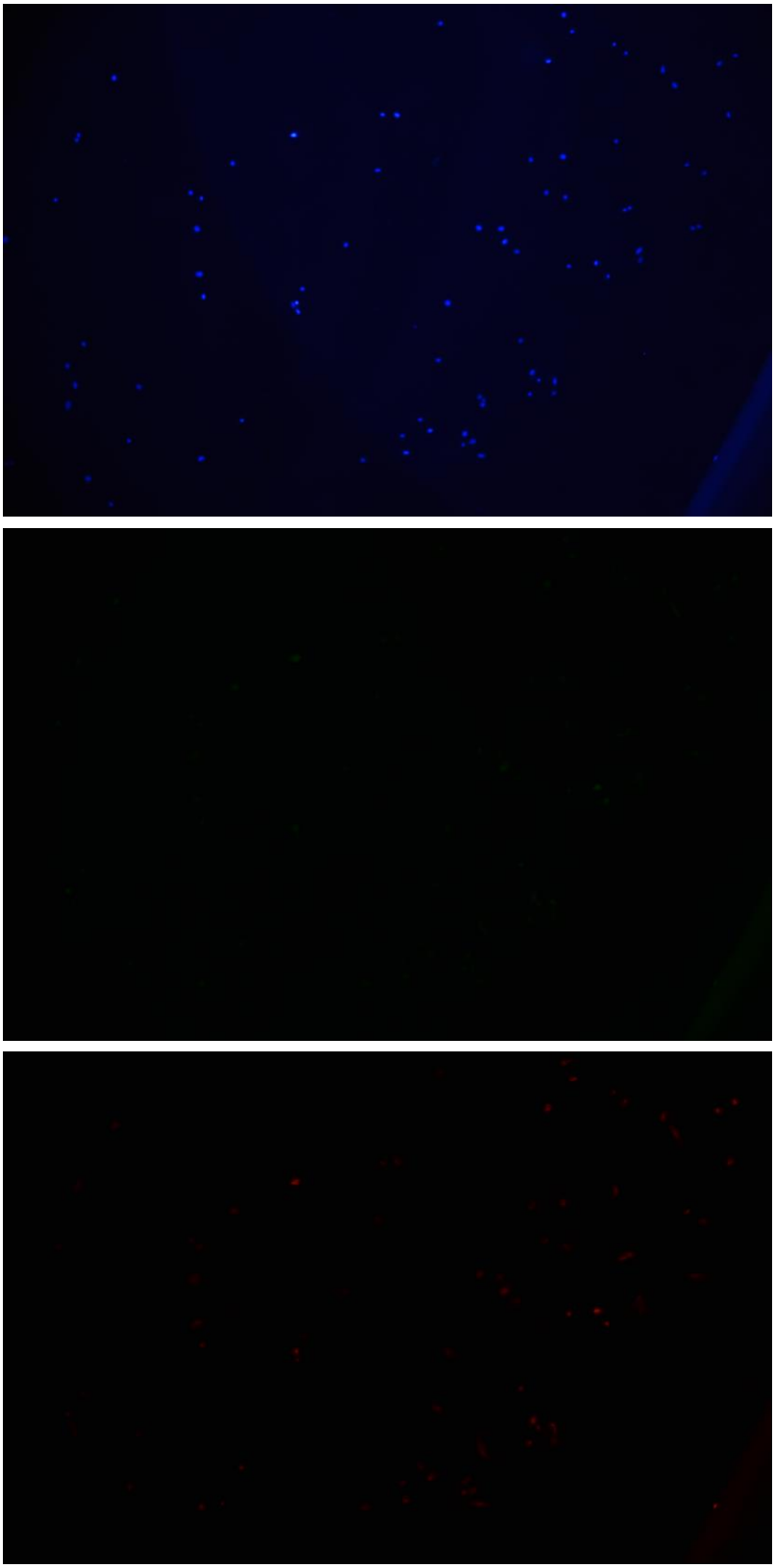

Figure 20. Immunostaining images of M2 control group at 72 hours of macrophage polarization at x100 zoom.

In Figures 21, 22 and 23. it is possible to observe the nucleus of the cells in the blue filtered images throughout days 1 to 3. In Day 1, in the blue filtered image one can observe many cells, whereas there are less observable cells in the green filtered image and even less in the red-filtered image. In day 2, one can observe less cells in the blue filtered image compared to day one, whereas in the green filtered image there are roughly as many cells as in day 1, but less cells in the red-filtered image than in day 1. In the final day, in the blue-filtered image, there seems to be even less cells than in day 2, whereas there seems to be the same amount of cells in the green-filtered image than in days 1 and 2, and it seems that there are more cells in the red-filtered image than days 1 and 2. This results mean that although there wasn't much polarization, most of it was into the M2 phenotype.

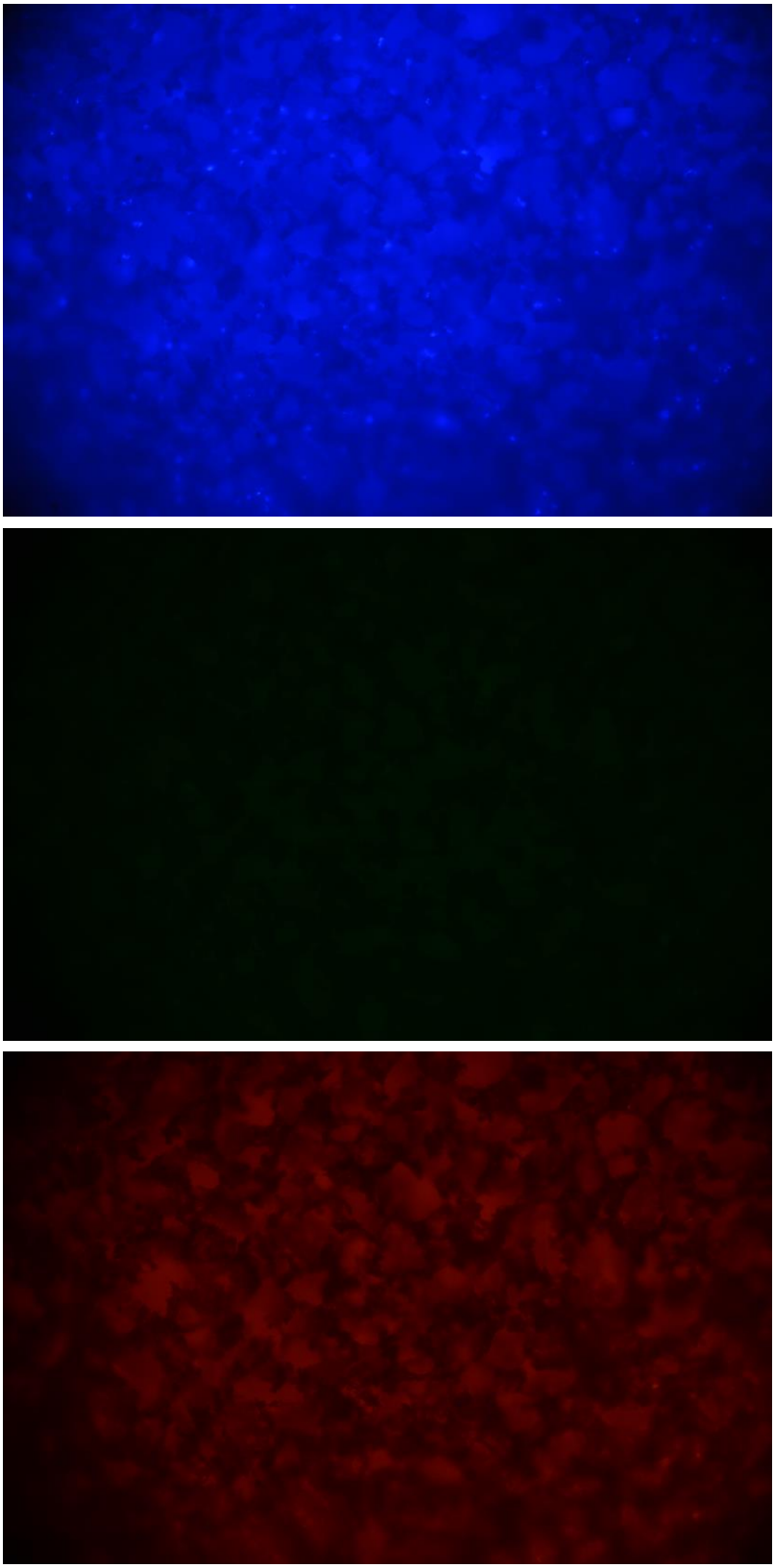

Figure 21. Immunostaining images of PCLs at 24 hours of macrophage polarization at x100 zoom.

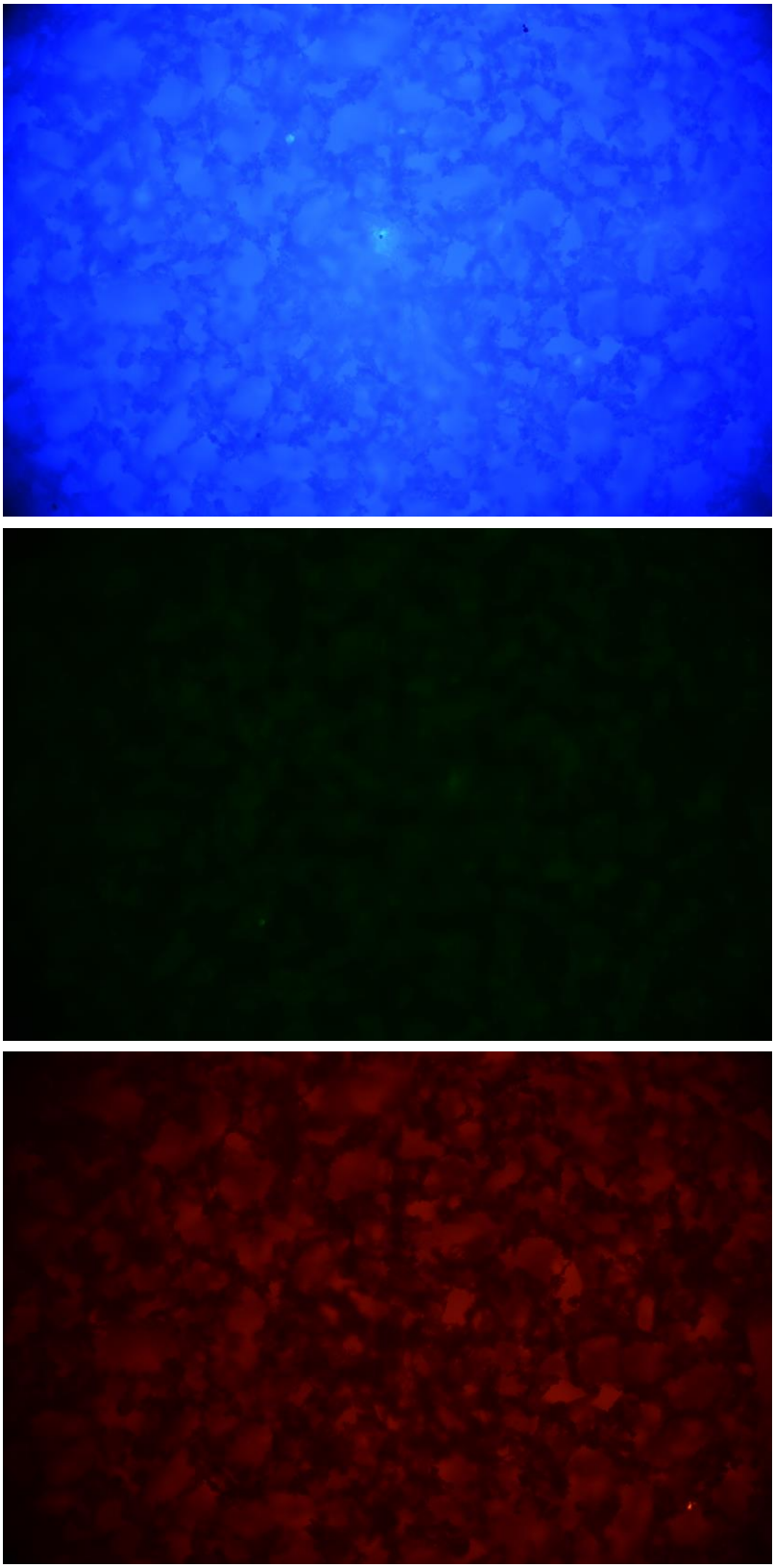

Figure 22. Immunostaining images of PCLs at 48 hours of macrophage polarization at x100 zoom.

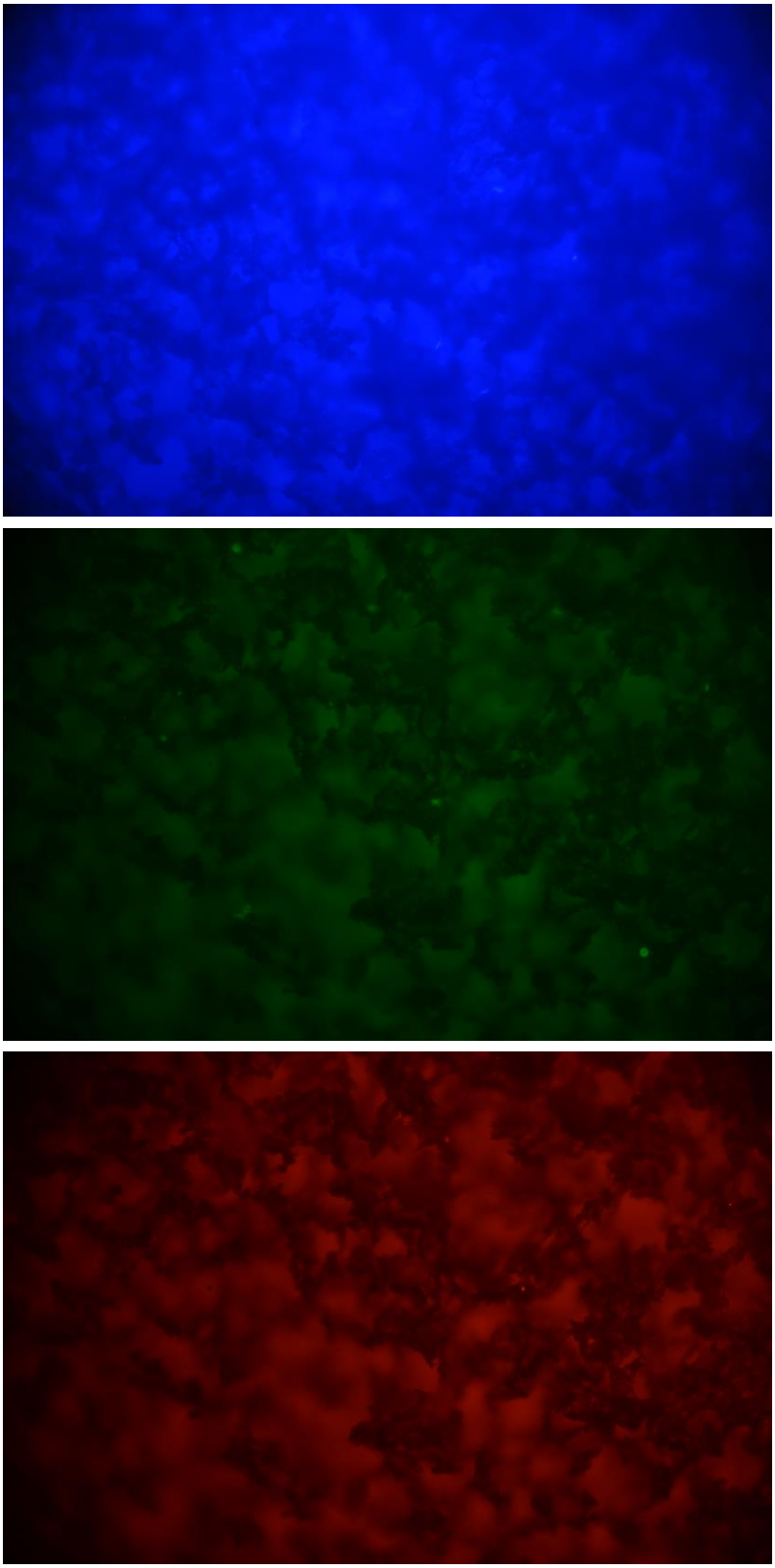

Figure 23. Immunostaining images of PCLs at 72 hours of macrophage polarization at x100 zoom.

In Figures 24, 25 and 26. it is possible to observe the nucleus of the cells in the blue filtered images throughout days 1 to 3. In Day 1, in the blue filtered image one can observe some cells, about the same ammount that are observable in the green filtered image, whereas there are none observable in the red-filtered image. In day 2, one can observe about the same ammount cells in the blue filtered image compared to day one, whereas in the green filtered image there are many more cells than in day 1 and they extremely well illuminated, but in the red-filtered image, like day 1, there are no observable cells. In the final day, in the blue-filtered image there seems to be about the same ammount of cells than in day 2, whereas there seems to be less cells in the green-filtered image than in day 2 but they are still very well observable, and it seems that there are once again, no observable cells in the red-filtered image. These results show that standard Bioglass-PCL scaffolds induce much more polarization into the M2 phenotype.

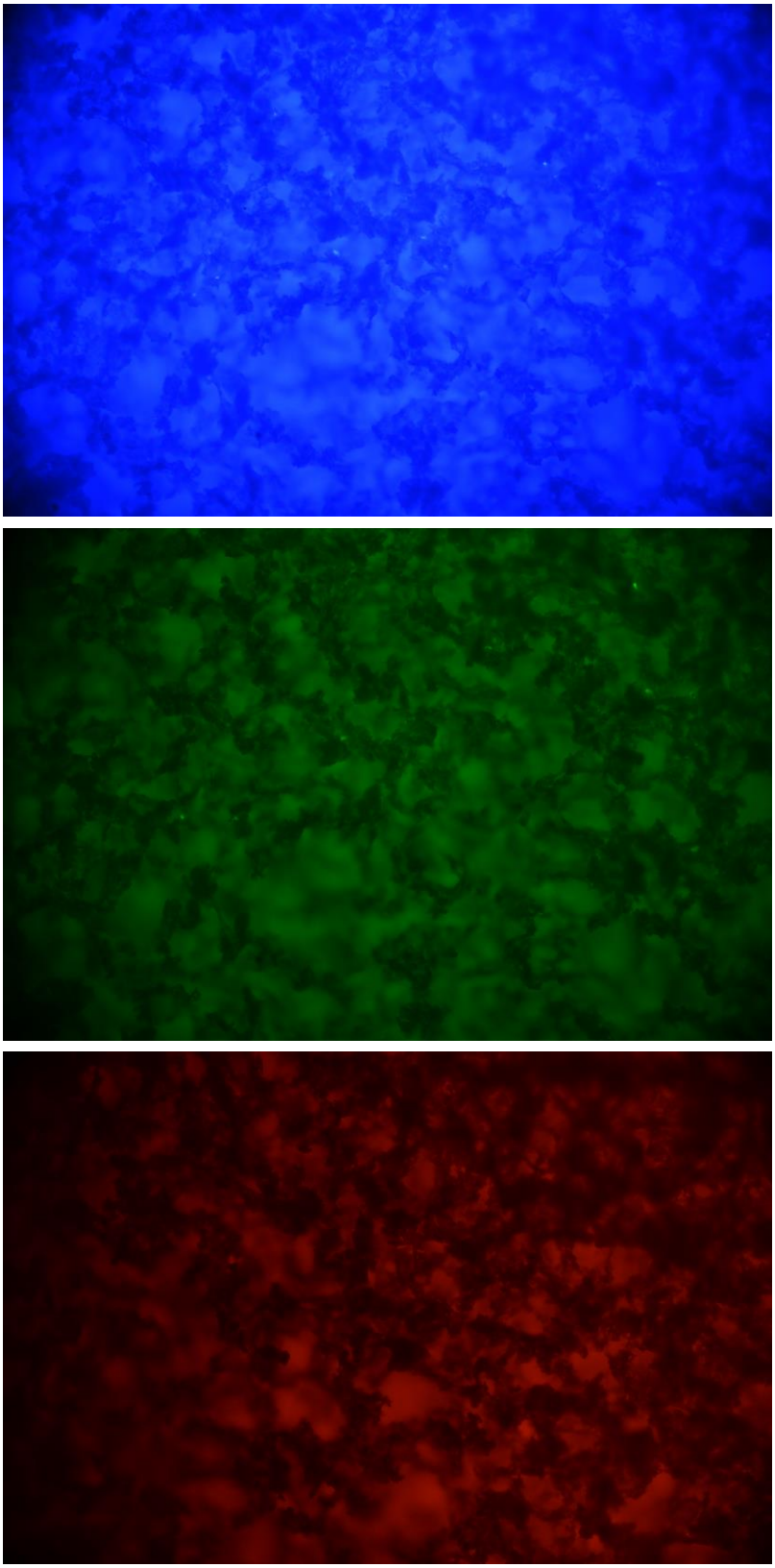

Figure 24. Immunostaining images of 45S5BGs at 24 hours of macrophage polarization at x100 zoom.

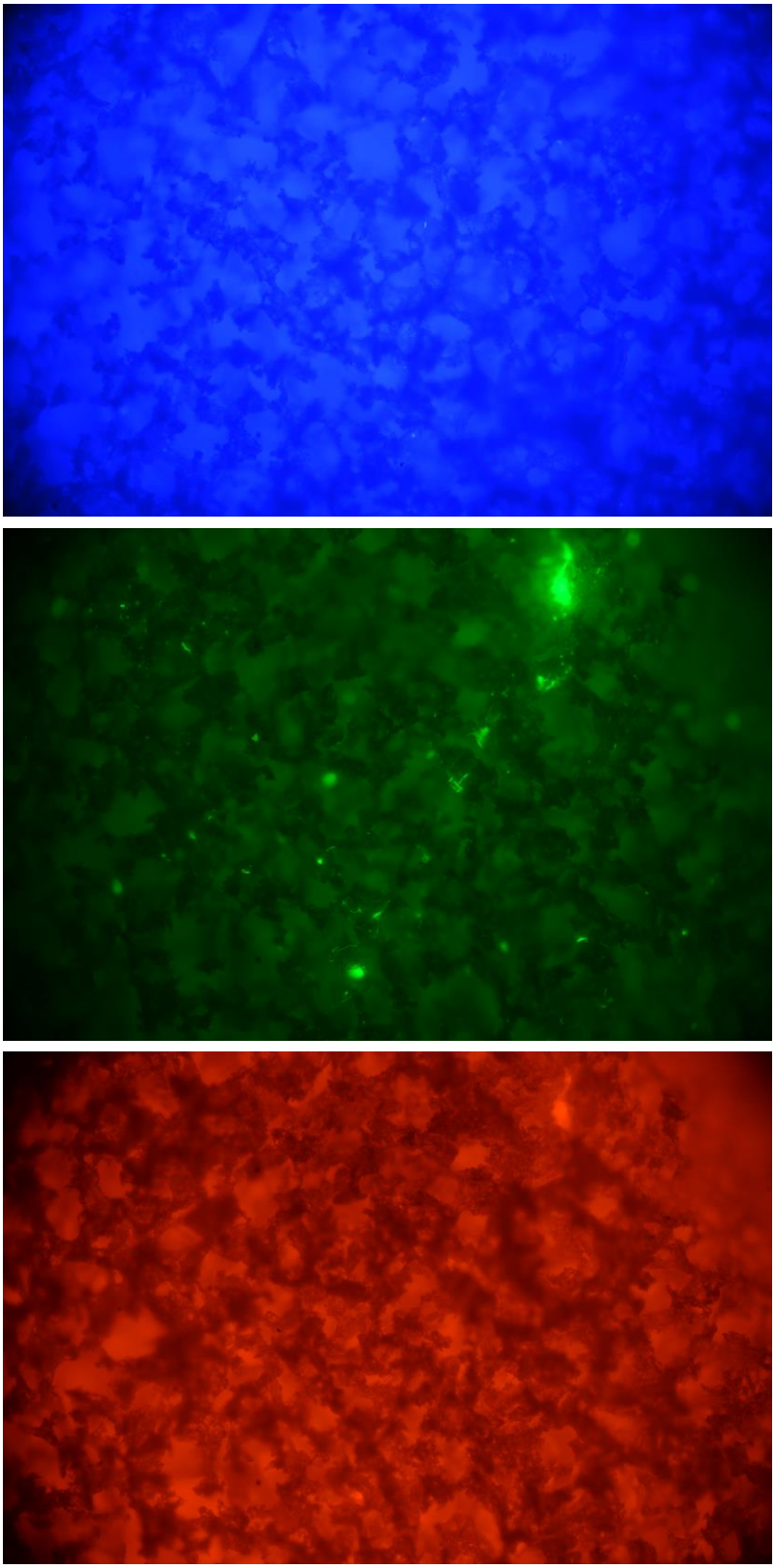

Figure 25. Immunostaining images of 45S5BGs at 48 hours of macrophage polarization at x100 zoom.

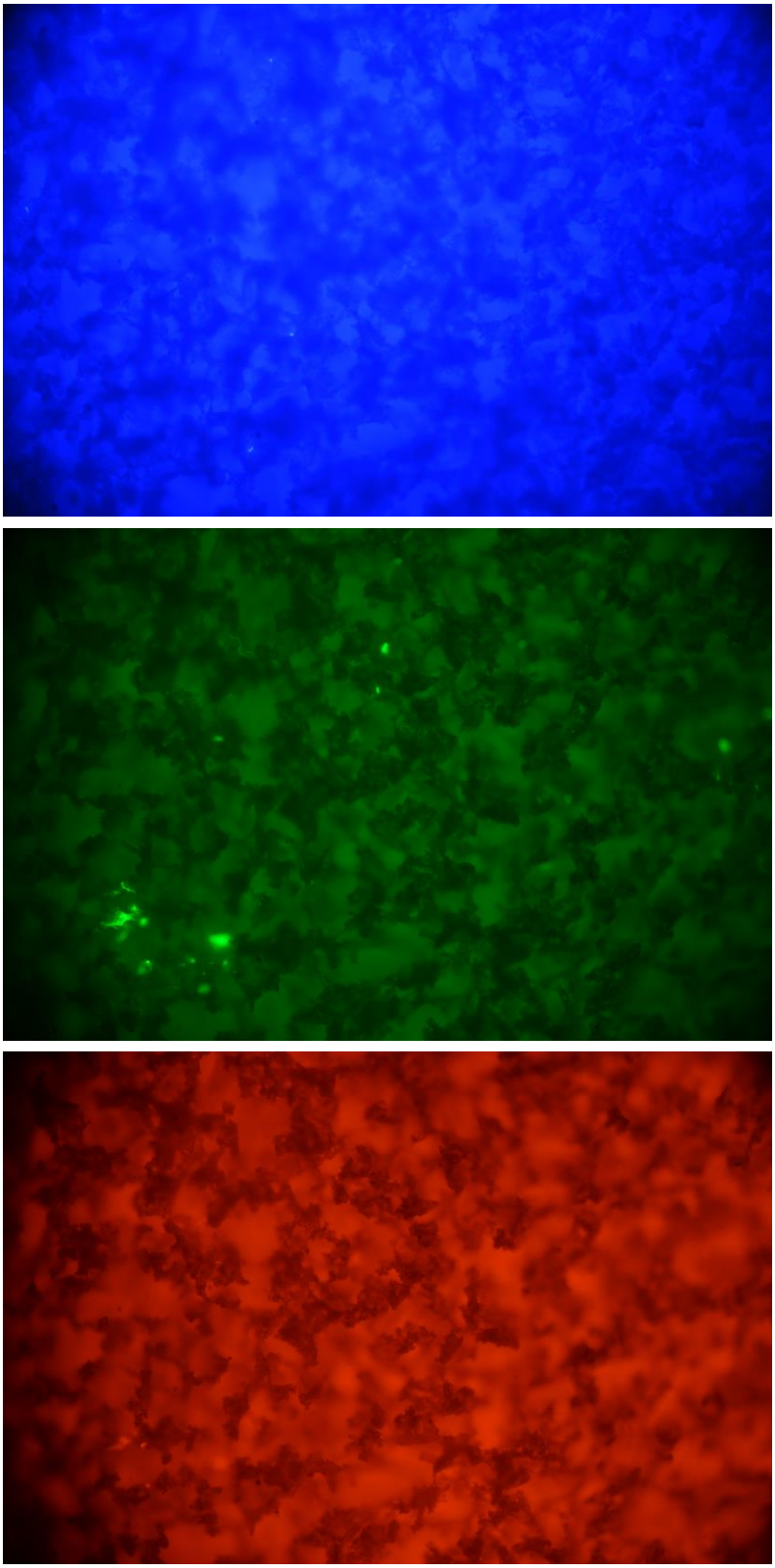

Figure 26. Immunostaining images of 45S5BGs at 72 hours of macrophage polarization at x100 zoom.

In Figures 27, 28 and 29. it is possible to observe the nucleus of the cells in the blue filtered images throughout days 1 to 3. In Day 1, in the blue filtered image one can observe some cells, whereas there are many observable and pronounced cells in the green filtered image, whilst there are no observable cells in the red-filtered image. In day 2, one can observe about the same ammount cells in the blue filtered image compared to day one, whereas in the green filtered image there is an abundance of cells, it still seems to be less cells than in day 1, and in the red-filtered image there are still no observable cells. In the final day, there seems to be more cells present than in day 2, whereas there seems to be even less cells in the green-filtered image than in days 1 and 2, whilst it seems that there is one observable cell in the red-filtered image. These results mean that the niobium-doped BG scaffolds induce polarization into the M2 phenotype.

These results show promise, but there should be more tests conducted, seeing as these results are from a single biological replicate, meaning that these results could deviate from each experiment done, since they do not have much statistical relevance, due to having been conducted with only one biological replicate.

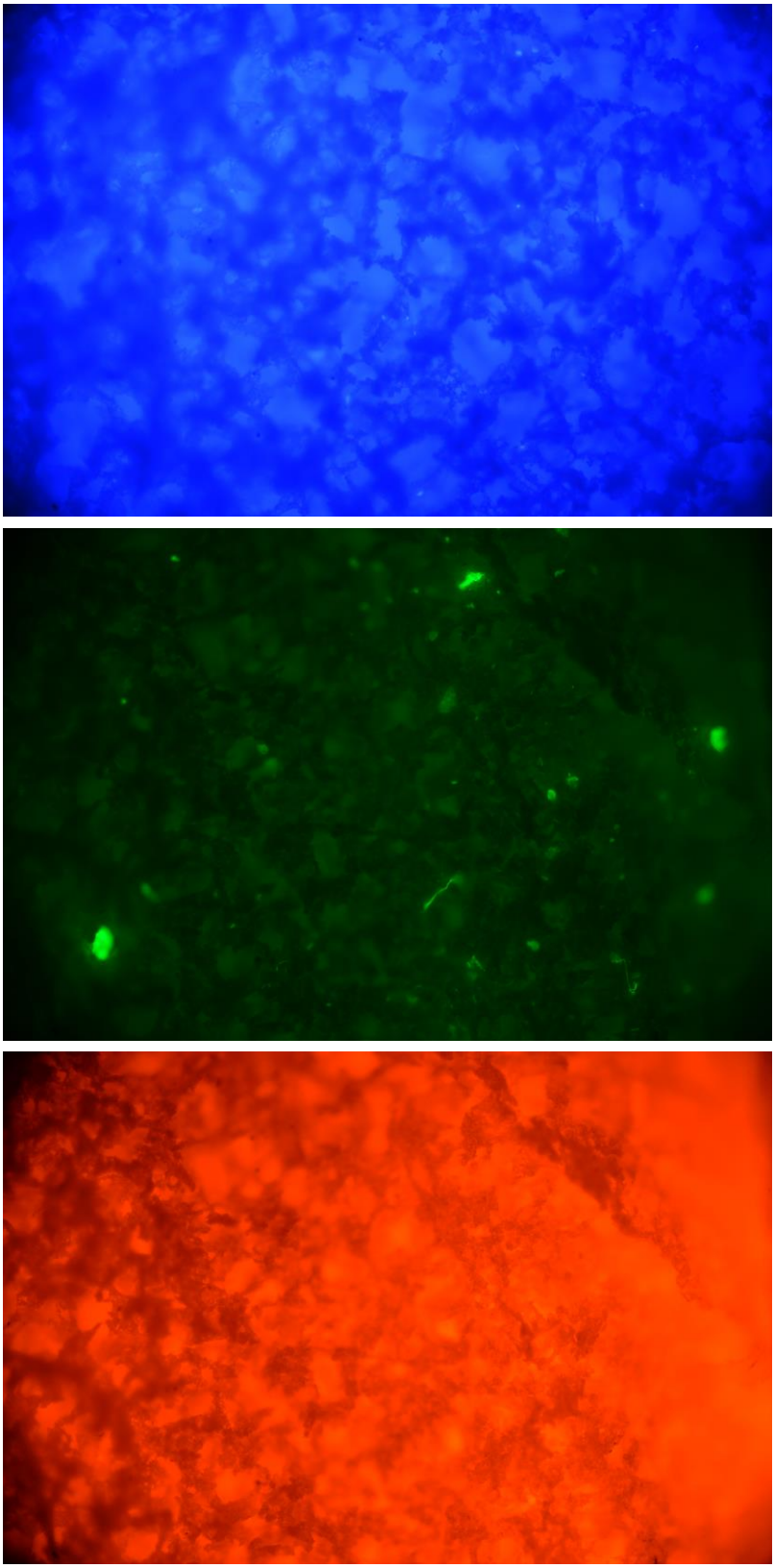

Figure 27. Immunostaining images of Nb4%BGs at 24 hours of macrophage polarization at x100 zoom.

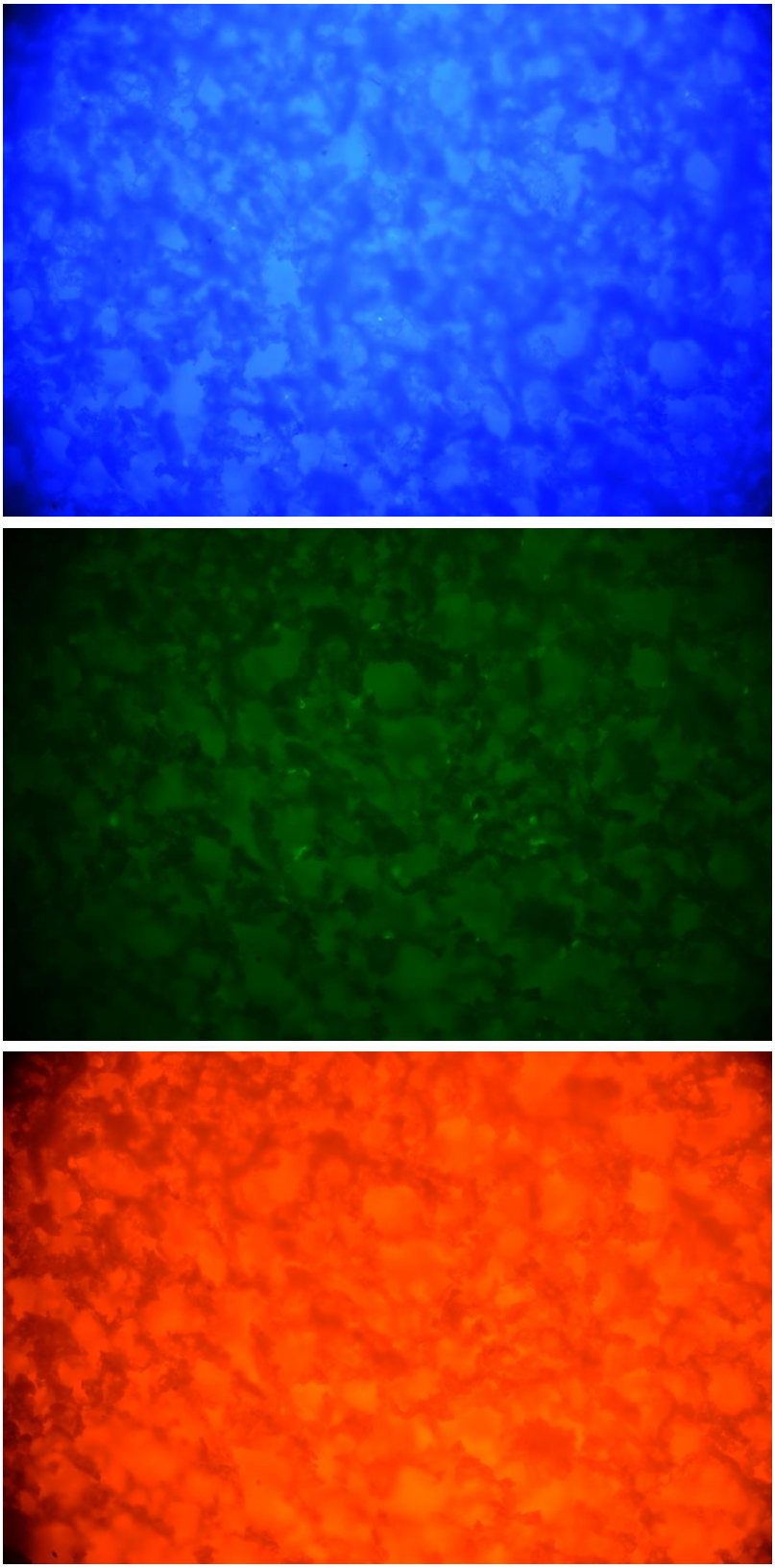

Figure 28. Immunostaining images of Nb4%BGs at 48 hours of macrophage polarization at x100 zoom.

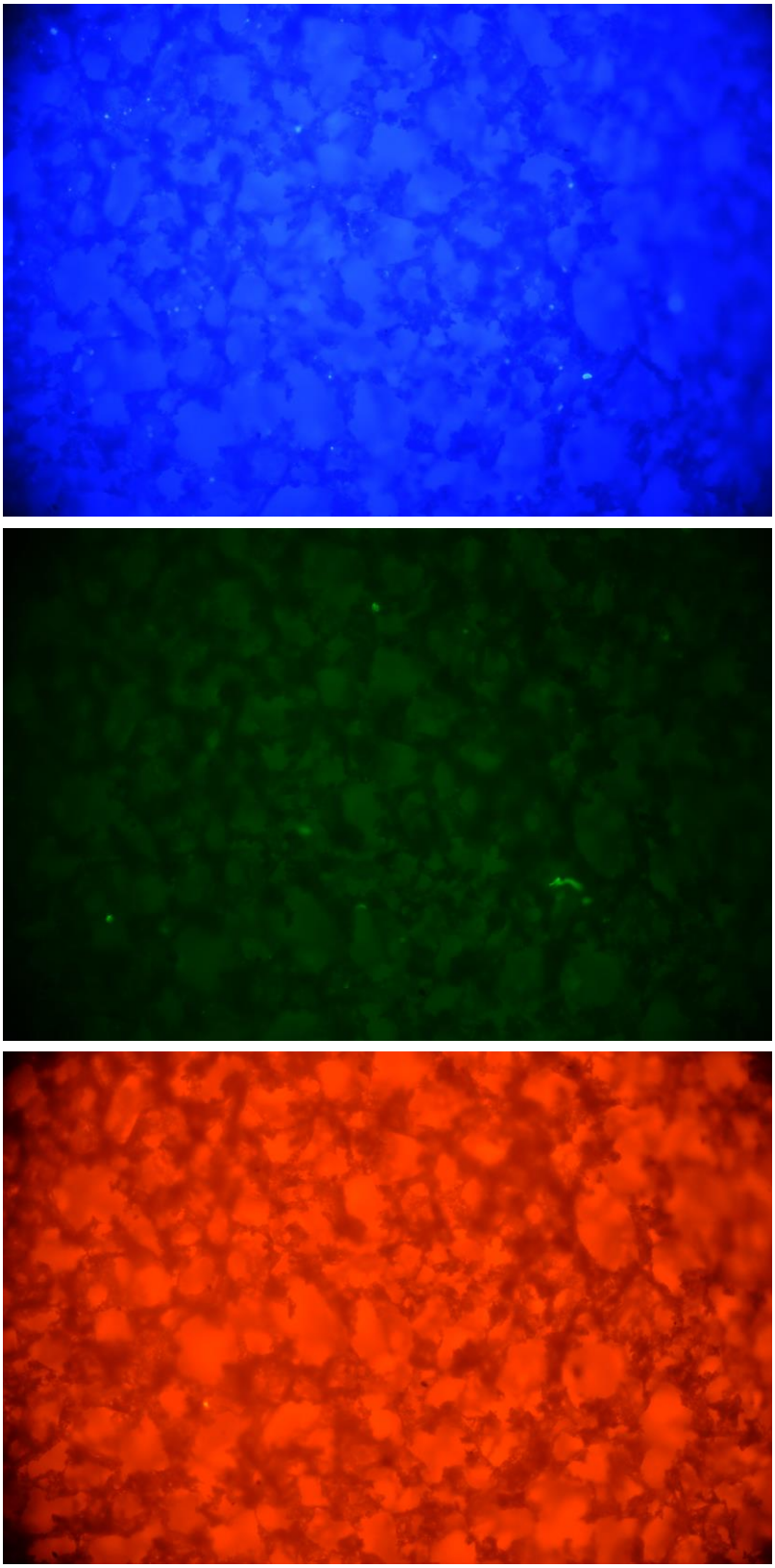

Figure 29. Immunostaining images of Nb4%BGs at 72 hours of macrophage polarization at x100 zoom.

4

CONCLUSION AND FUTURE PERSPECTIVES

Serious bone injuries are one of the most common and prevalent health issues worldwide that require improvements in treatment. In bone tissue engineering there have been attempts at developing scaffolds that enhance and promote bone regeneration by incorporating several osteogenic and osteoinductive compounds.

This thesis had the objective of taking a step toward solving this problem, by incorporating niobium-doped Bioglass® in a PCL scaffold, in order to induce M2 macrophage polarization and cell growth without inducing cytotoxicity. These scaffolds were successfully produced, having a porous network, with pore interconnectivity and a size around 140 μm, which is a size that promotes cell proliferation. It was also confirmed that the addition of niobium does not reciprocate in any sort of modification in the structure of the glass matrix. Through this work, it has also been made clear that passivation is a required step in order to achieve desirable levels of cell viability. These Nb4%BGs showed better cell viability and induced more ALP production than standard 45S5BGs and PCLs. But, in contrast, they showed less adhesion and proliferation than the PCLs, and none of the scaffolds presented any anti-bacterial effect. Both 45S5BGs and Nb4%BGs were shown to induce M2 macrophage polarization, whilst the PCLs did not induce much polarization. Further studies should be conducted to confirm if there is no anti-bacterial effect, and the ion release should be studied. There should be SEM images taken of the scaffolds throughout several points in time of them being immersed in SBF, in order to have a better understanding of the scaffold's structure and formation of the Ca/P layer. Further tests on macrophage polarization should also be conducted, seeing as this test was done with a single biological replicate.

BIBLIOGRAPHY

1. Stevens MM. *Biomaterials for Bone Tissue Engineering*.; 2008.
2. Pallua N, Suschek C V. *Tissue Engineering: From Lab to Clinic*. Vol 9783642028243. Springer-Verlag Berlin Heidelberg; 2011. doi:10.1007/978-3-642-02824-3
3. Amini AR, Laurencin CT, Nukavarapu SP. *Bone Tissue Engineering: Recent Advances and Challenges*.; 2012.
4. Meng Bao C Le, Y.L. E, S.K. M, Liu Y, Choolani M, K.Y. J. Advances in Bone Tissue Engineering. In: *Regenerative Medicine and Tissue Engineering*. InTech; 2013. doi:10.5772/55916
5. Fernandez-Yague MA, Abbah SA, McNamara L, Zeugolis DI, Pandit A, Biggs MJ. Biomimetic approaches in bone tissue engineering: Integrating biological and physicomechanical strategies. *Adv Drug Deliv Rev*. 2015;84:1-29. doi:10.1016/j.addr.2014.09.005
6. Glowacki J, Mizuno S. Collagen scaffolds for tissue engineering. *Biopolymers*. 2008;89(5):338-344. doi:10.1002/bip.20871
7. Sundelacruz S, Kaplan DL. Stem cell- and scaffold-based tissue engineering approaches to osteochondral regenerative medicine. *Semin Cell Dev Biol*. 2009;20(6):646-655. doi:10.1016/j.semcdb.2009.03.017
8. Rezwan K, Chen QZ, Blaker JJ, Boccaccini AR. Biodegradable and bioactive porous polymer/inorganic composite scaffolds for bone tissue engineering. *Biomaterials*. 2006;27(18):3413-3431. doi:10.1016/j.biomaterials.2006.01.039
9. Kim SS, Sun Park M, Jeon O, Yong Choi C, Kim BS. Poly(lactide-co-glycolide)/hydroxyapatite composite scaffolds for bone tissue engineering. *Biomaterials*. 2006;27(8):1399-1409. doi:10.1016/j.biomaterials.2005.08.016
10. Hutmacher DW, Schantz JT, Lam CXF, Tan KC, Lim TC. State of the art and future directions of scaffold-based bone engineering from a biomaterials perspective. *J Tissue Eng Regen Med*. 2007;1(4):245-260. doi:10.1002/term.24

11. Hutmacher DW. Scaffold design and fabrication technologies for engineering tissues - State of the art and future perspectives. *J Biomater Sci Polym Ed*. 2001;12(1):107-124. doi:10.1163/156856201744489
12. Mastrogiacomo M, Scaglione S, Martinetti R, et al. Role of scaffold internal structure on in vivo bone formation in macroporous calcium phosphate bioceramics. *Biomaterials*. 2006;27(17):3230-3237. doi:10.1016/j.biomaterials.2006.01.031
13. Unger RE, Wolf M, Peters K, Motta A, Migliaresi C, Kirkpatrick CJ. Growth of human cells on a non-woven silk fibroin net: A potential for use in tissue engineering. *Biomaterials*. 2004;25(6):1069-1075. doi:10.1016/S0142-9612(03)00619-7
14. Yu H, VandeVord PJ, Mao L, Matthew HW, Wooley PH, Yang SY. Improved tissue-engineered bone regeneration by endothelial cell mediated vascularization. *Biomaterials*. 2009;30(4):508-517. doi:10.1016/j.biomaterials.2008.09.047
15. Murphy WL, Simmons CA, Kaigler D, Mooney DJ. Bone regeneration via a mineral substrate and induced angiogenesis. *J Dent Res*. 2004;83(3):204-210. doi:10.1177/154405910408300304
16. Kaigler D, Wang Z, Horger K, Mooney DJ, Krebsbach PH. VEGF scaffolds enhance angiogenesis and bone regeneration in irradiated osseous defects. *Journal of Bone and Mineral Research*. 2006;21(5):735-744. doi:10.1359/jbmr.060120
17. Narayan D, Venkatraman SS. Effect of pore size and interpore distance on endothelial cell growth on polymers. *J Biomed Mater Res A*. 2008;87(3):710-718. doi:10.1002/jbm.a.31749
18. Karageorgiou V, Kaplan D. Porosity of 3D biomaterial scaffolds and osteogenesis. *Biomaterials*. 2005;26(27):5474-5491. doi:10.1016/j.biomaterials.2005.02.002
19. Siddiqui N, Kishori B, Rao S, et al. Electropsun Polycaprolactone Fibres in Bone Tissue Engineering: A Review. *Mol Biotechnol*. 2021;63(5):363-388. doi:10.1007/s12033-021-00311-0
20. Abedalwafa M, Wang F, Wang L, Li C. *Biodegradable Poly-Epsilon-Caprolactone (PCL) for Tissue Engineering Applications: A Review Biodegradable Poly-Epsilon-Caprolactone (PCL) for Tissue Engineering Applications: A Review Rev BIODEGRADABLE POLY-EPSILON-CAPROLACTONE (PCL) FOR TISSUE ENGINEERING APPLICATIONS: A REVIEW*. Vol 34.; 2013. https://www.researchgate.net/publication/265843722
21. Kim MS, Kim JH, Min BH, Chun HJ, Han DK, Lee HB. Polymeric scaffolds for regenerative medicine. *Polymer Reviews*. 2011;51(1):23-52. doi:10.1080/15583724.2010.537800
22. Bharadwaz A, Jayasuriya AC. Recent trends in the application of widely used natural and synthetic polymer nanocomposites in bone tissue regeneration. *Materials Science and Engineering C*. 2020;110. doi:10.1016/j.msec.2020.110698
23. Labet M, Thielemans W. Synthesis of polycaprolactone: A review. *Chem Soc Rev*. 2009;38(12):3484-3504. doi:10.1039/b820162p

24. Ibrahim SW, Hamad TI, Haider J. Biological properties of polycaprolactone and barium titanate composite in biomedical applications. *Sci Prog*. 2023;106(4). doi:10.1177/00368504231215942
25. Kumari A, Yadav SK, Yadav SC. Biodegradable polymeric nanoparticles based drug delivery systems. *Colloids Surf B Biointerfaces*. 2010;75(1):1-18. doi:10.1016/j.colsurfb.2009.09.001
26. Hench LL. The story of Bioglass®. In: *Journal of Materials Science: Materials in Medicine*. Vol 17. ; 2006:967-978. doi:10.1007/s10856-006-0432-z
27. Gavinho SR, Pádua AS, Sá-Nogueira I, et al. Fabrication, Structural and Biological Characterization of Zinc-Containing Bioactive Glasses and Their Use in Membranes for Guided Bone Regeneration. *Materials*. 2023;16(3). doi:10.3390/ma16030956
28. Taye MB. Biomedical applications of ion-doped bioactive glass: a review. *Applied Nanoscience (Switzerland)*. 2022;12(12):3797-3812. doi:10.1007/s13204-022-02672-7
29. Hammami I, Gavinho SR, Pádua AS, et al. Extensive Investigation on the Effect of Niobium Insertion on the Physical and Biological Properties of 45S5 Bioactive Glass for Dental Implant. *Int J Mol Sci*. 2023;24(6). doi:10.3390/ijms24065244
30. Jones JR. Reprint of: Review of bioactive glass: From Hench to hybrids. *Acta Biomater*. 2015;23(S):S53-S82. doi:10.1016/j.actbio.2015.07.019
31. Oliver J anne N, Su Y, Lu X, Kuo PH, Du J, Zhu D. Bioactive glass coatings on metallic implants for biomedical applications. *Bioact Mater*. 2019;4:261-270. doi:10.1016/j.bioactmat.2019.09.002
32. Gavinho SR, Pádua AS, Sá-Nogueira I, et al. Biocompatibility, Bioactivity, and Antibacterial Behaviour of Cerium-Containing Bioglass®. *Nanomaterials*. 2022;12(24). doi:10.3390/nano12244479
33. Pantulap U, Arango-Ospina M, Boccaccini AR. Bioactive glasses incorporating less-common ions to improve biological and physical properties. *J Mater Sci Mater Med*. 2022;33(1). doi:10.1007/s10856-021-06626-3
34. Thompson KH, Orvig C. *60. C. Rensing, B. Mitra, B. P. Rosen*. Vol 8.; 2003. http://science.sciencemag.org/
35. Spadair JA, Becker RO, Bachman CH. *By Springer-Verlag 1970 Public Health Service and by the Veterans Administration Research Service. 4 Calc*. Vol 6.; 1970.
36. Holloway EM, Wu JH, Czerwinski M, et al. Differentiation of Human Intestinal Organoids with Endogenous Vascular Endothelial Cells. *Dev Cell*. 2020;54(4):516-528.e7. doi:10.1016/j.devcel.2020.07.023
37. Denry IL, Holloway JA, Nakkula RJ, Walters JD. Effect of niobium content on the microstructure and thermal properties of fluorapatite glass-ceramics. *J Biomed Mater Res B Appl Biomater*. 2005;75(1):18-24. doi:10.1002/jbm.b.30295

38. Lopes JH, Souza LP, Domingues JA, et al. In vitro and in vivo osteogenic potential of niobium-doped 45S5 bioactive glass: A comparative study. *J Biomed Mater Res B Appl Biomater*. 2020;108(4):1372-1387. doi:10.1002/jbm.b.34486
39. Miguez-Pacheco V, de Ligny D, Schmidt J, Detsch R, Boccaccini AR. Development and characterization of niobium-releasing silicate bioactive glasses for tissue engineering applications. *J Eur Ceram Soc*. 2018;38(3):871-876. doi:10.1016/J.JEURCERAMSOC.2017.07.028
40. Hohenbild F, Arango-Ospina M, Moghaddam A, Boccaccini AR, Westhauser F. Preconditioning of bioactive glasses before introduction to static cell culture: What is really necessary? *Methods Protoc*. 2020;3(2):1-12. doi:10.3390/mps3020038
41. Thavornyutikarn B, Feltis B, Wright PFA, Turney TW. Effect of pre-treatment of crystallized bioactive glass with cell culture media on structure, degradability, and biocompatibility. *Materials Science and Engineering C*. 2019;97:188-197. doi:10.1016/j.msec.2018.12.034
42. Pryce RS, Hench LL. Dissolution characteristics of bioactive glasses. In: *Key Engineering Materials*. Vol 240-242. Trans Tech Publications Ltd; 2003:201-204. doi:10.4028/www.scientific.net/kem.240-242.201
43. El-Rashidy AA, Roether JA, Harhaus L, Kneser U, Boccaccini AR. Regenerating bone with bioactive glass scaffolds: A review of in vivo studies in bone defect models. *Acta Biomater*. 2017;62:1-28. doi:10.1016/j.actbio.2017.08.030
44. Wang N, Liang H, Zen K. Molecular mechanisms that influence the macrophage M1-M2 polarization balance. *Front Immunol*. 2014;5(NOV). doi:10.3389/fimmu.2014.00614
45. Dijkgraaf EM, Heusinkveld M, Tummers B, et al. Chemotherapy alters monocyte differentiation to favor generation of cancer-supporting m2 macrophages in the tumor microenvironment. *Cancer Res*. 2013;73(8):2480-2492. doi:10.1158/0008-5472.CAN-12-3542
46. Fujiwara N, Kobayashi K. *Macrophages in Inflammation*. Vol 4.; 2005.
47. Allavena P, Sica A, Solinas G, Porta C, Mantovani A. The inflammatory micro-environment in tumor progression: The role of tumor-associated macrophages. *Crit Rev Oncol Hematol*. 2008;66(1):1-9. doi:10.1016/j.critrevonc.2007.07.004
48. Gordy C, Pua H, Sempowski GD, He YW. Regulation of steady-state neutrophil homeostasis by macrophages. Published online 2011. doi:10.1182/blood-2010-01
49. Oishi Y, Manabe I. Macrophages in inflammation, repair and regeneration. doi:10.1093/intimm/dxy054/5079207
50. Wynn TA, Chawla A, Pollard JW. Macrophage biology in development, homeostasis and disease. *Nature*. 2013;496(7446):445-455. doi:10.1038/nature12034
51. Dugan . L L, Choi DW. *Requirement of DNase II for Definitive Erythropoiesis in the Mouse Fetal Liver*. Vol 348.; 1993. www.sciencemag.org

52. Sindrilaru A, Peters T, Wieschalka S, et al. An unrestrained proinflammatory M1 macrophage population induced by iron impairs wound healing in humans and mice. *Journal of Clinical Investigation*. 2011;121(3):985-997. doi:10.1172/JCI44490
53. Orecchioni M, Ghosheh Y, Pramod AB, Ley K. Macrophage polarization: Different gene signatures in M1(Lps+) vs. Classically and M2(LPS-) vs. Alternatively activated macrophages. *Front Immunol*. 2019;10(MAY). doi:10.3389/fimmu.2019.01084
54. Simunovic F, Finkenzeller G. Vascularization strategies in bone tissue engineering. *Cells*. 2021;10(7). doi:10.3390/cells10071749
55. Boccaccini AR, Chen Q, Lefebvre L, Gremillard L, Chevalier J. Sintering, crystallisation and biodegradation behaviour of Bioglass®-derived glass-ceramics. *Faraday Discuss*. 2007;136:27-44. doi:10.1039/b616539g
56. Ibrahim NF, Mohamad H, Mohd Noor SNF, Ahmad N. Melt-derived bioactive glass based on SiO2-CaO-Na2O-P2O5 system fabricated at lower melting temperature. *J Alloys Compd*. 2018;732:603-612. doi:10.1016/j.jallcom.2017.10.235
57. Ibrahim NF, Mohamad H, Mohd Noor SNF. Characterization on melt-derived bioactive glass powder from SiO2-CaO-Na2O-P2O5 system. *J Non Cryst Solids*. 2017;462:23-31. doi:10.1016/j.jnoncrysol.2017.01.040
58. Dziadek M, Zagrajczuk B, Jelen P, Olejniczak Z, Cholewa-Kowalska K. Structural variations of bioactive glasses obtained by different synthesis routes. *Ceram Int*. 2016;42(13):14700-14709. doi:10.1016/j.ceramint.2016.06.095
59. Schmitz SI, Widholz B, Essers C, et al. Superior biocompatibility and comparable osteoinductive properties: Sodium-reduced fluoride-containing bioactive glass belonging to the CaO–MgO–SiO2 system as a promising alternative to 45S5 bioactive glass. *Bioact Mater*. 2020;5(1):55-65. doi:10.1016/j.bioactmat.2019.12.005
60. Brito AF, Antunes B, dos Santos F, Fernandes HR, Ferreira JMF. Osteogenic capacity of alkali-free bioactive glasses. In vitro studies. *J Biomed Mater Res B Appl Biomater*. 2017;105(8):2360-2365. doi:10.1002/jbm.b.33771
61. Karadjian M, Essers C, Tsitlakidis S, et al. Biological properties of calcium phosphate bioactive glass composite bone substitutes: Current experimental evidence. *Int J Mol Sci*. 2019;20(2). doi:10.3390/ijms20020305
62. Hench LL, Jones JR, Sepulveda P. *Bioactive Materials for Tissue Engineering Scaffolds*. www.worldscientific.com
63. Miyazaki T, Kim HM, Kokubo T, Ohtsuki C, Nakamura T. *Apatite-Forming Ability of Niobium Oxide Gels in a Simulated Body Fluid*. Vol 109.; 2001.
64. Miyazaki T, Kim HM, Kokubo T, Kato H, Nakamura N, Ohtsuki C. Bonelike apatite formation on niobium oxide gel in a simulated body fluid. *Key Eng Mater*. 2001;192-195:43-46. doi:10.4028/www.scientific.net/kem.192-195.43

65. Ward LP, Strafford KN, Wilks TP, Subramanian C. *Materials Processing Technology THE ROLE OF REFRACTORY ELEMENT BASED COATINGS ON THE TRIBOLOGICAL AND BIOLOGICAL BEHAVIOUR OF ORTHOPAEDIC IMPLANTS*. Vol 56.; 1996.
66. Tamai M, Isama K, Nakaoka R, Tsuchiya T. Synthesis of a novel β-tricalcium phosphate/hydroxyapatite biphasic calcium phosphate containing niobium ions and evaluation of its osteogenic properties. *Journal of Artificial Organs*. 2007;10(1):22-28. doi:10.1007/s10047-006-0363-y
67. Capanema NSV, Mansur AAP, Carvalho SM, Silva ARP, Ciminelli VS, Mansur HS. Niobium-doped hydroxyapatite bioceramics: Synthesis, characterization and In Vitro cytocompatibility. *Materials*. 2015;8(7):4191-4209. doi:10.3390/ma8074191
68. Obata A, Takahashi Y, Miyajima T, Ueda K, Narushima T, Kasuga T. Effects of niobium ions released from calcium phosphate invert glasses containing Nb 2O 5 on osteoblast-like cell functions. *ACS Appl Mater Interfaces*. 2012;4(10):5684-5690. doi:10.1021/am301614a